IDENTIFYING FACTORS CONTROLLING CELL SHAPE AND VIRULENCE GENE EXPRESSION IN *BORRELIA BURGDORFERI*

Amberly Nicole Grothe

Submitted to the faculty of the University Graduate School
in partial fulfillment of the requirements
for the degree
Master of Science
in the Department of Microbiology and Immunology,
Indiana University

August 2019

Accepted by the Graduate Faculty of Indiana University, in partial fulfillment of the requirements for the degree of Master of Science.

Master's Thesis Committee

____

X. Frank Yang, Ph.D. - Chair

____

Stacey Gilk, Ph.D.

____

David Nelson, Ph.D.

ACKNOWLEDGEMENTS

There are many people without whom this work would not be possible. An endeavor like this is not one to be done without inspiration, without motivation, or without determination. To all of those who have encouraged me and supported me on my scientific journey, thank you.

To my parents and James, thank you for constantly pushing me forward and for believing in me even when I didn’t believe in myself. Your love and encouragement kept me stable and kept me motivated.

To my fellow lab members, thank you for your collaboration and your patience. Thank you for fulfilling the roles as friends, coworkers, and teachers all at once. And thank you to DJ and Sajith, whose troubleshooting work helped me tremendously.

Thank you to my committee members, Dr. Stacey Gilk and Dr. David Nelson, for your advice and your insight. Thank you for motivating me and helping to guide my project alongside my mentor.

And to my mentor, Dr. Frank Yang, thank you for all the help and guidance you provided throughout my time in the lab. Despite numerous fallbacks, you never said an unkind word and you always motivated us to keep going, to keep trying. Your patience and encouragement have been invaluable to me.

And last but most importantly, I would like to thank God for blessing me with this opportunity to learn and grow, both as a scientist and a person, and for giving me the strength to persevere when times got tough. It is through Him that all things are possible.

Amberly Nicole Grothe

IDENTIFYING FACTORS CONTROLLING CELL SHAPE AND VIRULENCE GENE EXPRESSION IN *BORRELIA BURGDORFERI*

Lyme disease is a multi-system inflammatory disorder that is currently the fastest growing arthropod-borne disease in the United States. The Lyme disease pathogen, *Borrelia burgdorferi*, exists within an enzootic cycle consisting of *Ixodes* tick vectors and a variety of vertebrate hosts. *Borrelia* lies within a distinct clade of microorganisms known as spirochetes which exhibit a unique spiral morphology. The underlying genetic mechanisms controlling for borrelial morphologies are still being discovered. One flagellar protein, FlaB, has been indicated to affect both spiral shape and motility of the organisms and significantly impacts the organism's ability to establish infection. Due to the potential connection between morphological characteristics and pathogenesis, we sought to screen and identify morphological mutants in an attempt to identify genes associated with morphological phenotypes of *Borrelia burgdorferi*.

Among *Borrelia*'s unique features is the presence of abundant lipoproteins making up its cellular membrane as opposed to the typical lipopolysaccharides. These proteins confer a wide variety of functions to the microorganism, among which include the abilities to circulate between widely differing hosts and to establish infection. Two important outer surface proteins, OspC and OspA, are found to be inversely expressed throughout the borrelial life cycle. OspC, in particular, becomes highly expressed during tick-feeding and transmission to the mammalian host. It has been found to be essential for establishment of infection. A global regulatory pathway has been shown to control for OspC, however there are missing links in this pathway between the external stimuli (such as temperature, pH, and cell density) and the regulatory pathway. We have performed a screening process to identify OspC expression mutants in order to identify novel genes associated with this pathway.

X. Frank Yang, Ph.D. - Chair

TABLE OF CONTENTS

LIST OF TABLES

LIST OF FIGURES

LIST OF ABBREVIATIONS

BadP – Borrelia host adaptation protein

BadR – Borrelia host adaptation regulator

BosR – Borrelia oxidative stress regulator

BSK – Barbour-Stoenner Kelly

CDC – Center for Disease Control

CheA – Chemotaxis protein CheA

CheB – Chemotaxis protein CheB

CheR – Chemotaxis protein methyltransferase

CheW – Chemotaxis protein CheW

CheX – Chemotaxis protein CheX

CheY – Chemotaxis protein CheY

Cp – Circular plasmid

Cpf – Cells per field

CsrA – Carbon storage regulator A

DbpA – Decorin-binding protein A

DhhP – DHH-DHHA1 domain protein

ECM – Erythema Chronicum Migrans

EM – Erythema Migrans

FlaA – Flagellin A

FlaB – Flagellin B

FlgE – Flagellar hook protein FlgE

FliF – Flagellar M-ring protein

FliG2 – Flagellar motor switch protein

Gen – Gentamycin

Hfq – RNA chaperone protein

Kan - Kanamycin

Kb – Kilobases

LB – Luria-Bertani (media)

Lp – Linear plasmid

LuxS – S-ribosylhomocysteine lyase

MCP – Methyl-accepting Chemotaxis Protein

MotA – Motility protein A

MotB – Motility protein B

OspA – Outer Surface Protein A

OspC – Outer Surface Protein C

PBS – Phosphate buffered saline

pGKT – plasmid Gentamycin Kanamycin Transposase

PTLD – Post-Treatment Lyme Disease

ResT – Telomere resolvase ResT

RpoN – Alternative sigma factor 54

RpoS – Alternative sigma factor S

Rrp2 – Response regulatory protein 2

SD – Standard Deviation

SDS – Sodium Dodecyl Sulfate

SDS-PAGE – Sodium Dodecyl Sulfate-Polyacrylamide Gel Electrophoresis

Tn - Transposon

Wt – Wild-type

INTRODUCTION

Lyme Disease History

Lyme disease is a multi-system inflammatory disorder that is currently the fastest growing vector-borne disease in the U.S. Lyme disease was initially recognized in Lyme, Connecticut in 1976 when a large incidence of children was found exhibiting symptoms of juvenile arthritis. The occurrence of the characteristic bulls-eye rash now associated with Lyme disease was apparent in 25% percent of the cases (Steere *et al*, 1977). This led to an investigation of the disease, with the hypothesis that it was caused by an infectious agent. Due to the increased prevalence of this disease in rural, wooded areas, it was further hypothesized that the clinical agent may be transmitted via an arthropod vector (Steere *et al*, 1978). Six years later, in 1982, spirochetal bacteria were isolated from the midgut of an *Ixodes* tick by Willy Burgdorfer and his research team. At this point, *Borrelia burgdorferi* was identified as the disease-causing pathogen (Burgdorfer *et al*, 1982).

The principal species responsible for infection in the US is *Ixodes scapularis*, formerly known as *Ixodes dammini*, which is responsible for the transmission of disease in the Northeastern and Upper Midwestern regions of the U.S. Milder forms of Lyme disease may be found on the western coast, which are caused by *Ixodes pacificus* (Schmid, 1985) (Figure 1.1A, 1.1B). A dramatic geographical expansion of reported Lyme disease cases, particularly in the Northeast and Midwestern regions, can be seen in Figures 1.1A and 1.1B. Lyme disease also occurs in Europe and parts of Asia and Africa, with *I. persulcatus* the major tick vector in Eastern Europe and Asia and *I. ricinus* a major vector in Northern Europe and Africa (Gray, 1998).

The initial incidence of Lyme disease in the United States was low but as knowledge of the disease expanded and detection methods improved, the reports of the disease have markedly increased. Lyme disease became a reportable disease in the U.S. in 1991 with an original incidence of 9465 cases per year. Over the last 30 years, incidence rates have nearly tripled with approximately 30,000 confirmed cases in 2017 (Figure 1.1C). Additionally, two studies performed by the CDC suggest that that Lyme disease diagnoses may be closer to 300,000 per year (CDC, 2018).

A

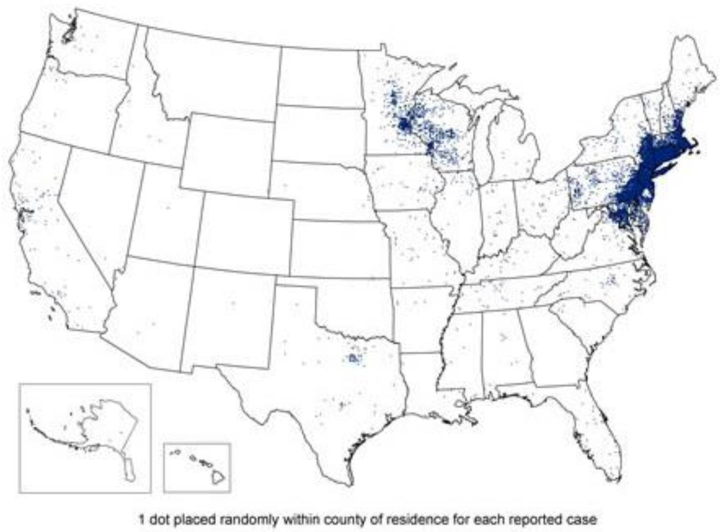
1 dot placed randomly within county of residence for each reported case

B

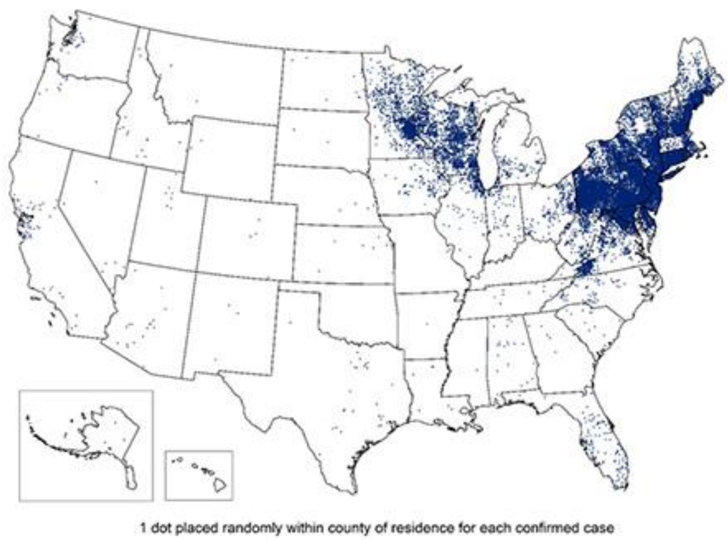
1 dot placed randomly within county of residence for each confirmed case

C

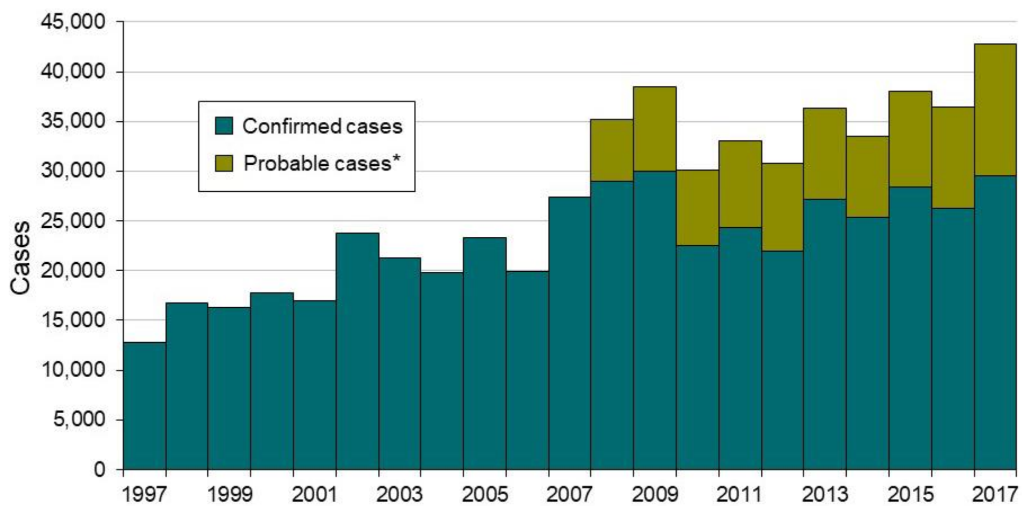
45,000
40,000
35,000
30,000
25,000
20,000
15,000
10,000
5,000
0
Cases
Confirmed cases
Probable cases*
1997
1999
2001
2003
2005
2007
2009
2011
2013
2015
2017

Figure 1.1: Incidence of Lyme Disease from 1997 to 2017

A, geographical incidence of Lyme Disease by county of residence in 2001. B, geographical incidence of Lyme Disease by county of residence in 2017. C, confirmed and probable cases reported per year to CDC from 1997 to 2017.

Source: CDC Lyme disease maps – Historical data; CDC Lyme disease chart and figures – Historical data

Stages, Symptoms, and Treatments

There are three defined stages of the infection. The initial stage of the disease is characterized by a localized infection found at the site of the tick bite. This stage typically presents as a characteristic bulls-eye rash, known as erythema migrans (EM) and flu-like symptoms. The next stage of the infection is disseminated infection, which occurs when the bacteria has spread to the circulatory system. Symptoms of this stage include secondary erythema migrans, which arises in areas of the body unassociated with tick bite site, and flu-like symptoms. If left untreated, Borrelia can localize into many different organs throughout the body. This stage is referred to as late or persistent infection and most commonly results in Lyme arthritis (Wright *et al*, 2012). However, rarer and more severe symptoms can occur such as myocarditis and neuroencephalitis (Burgdorfer, 1991; CDC, 2018; Cooke and Dattwyler, 1992; Steere, 2001; Steere *et al*, 2004).

Treatment is available for Lyme disease. This is typically an intense antibiotic regimen consisting of Doxycycline, Amoxicillin, and/or Cefuroxime axetil. Antibiotics usually are taken for several weeks/months (CDC, 2018). However, another rare stage can occur, known as Post-Treatment Lyme Disease syndrome or Chronic Lyme disease, in which recurring Lyme disease symptoms appear in patients who have already undergone Lyme disease treatment (Marques, 2008; Steere *et al*, 2004). Little is known about this syndrome and studies are currently being done to understand it.

Phylum *Spirochaetes* and the *Borrelia* genus

Borrelia burgdorferi lies within the family *Spirochaetes*, a unique and phylogenetically distinct group of bacteria. This family contains the well-known pathogens *Treponema pallidum*, the causative agent of syphilis, and *Leptospira interrogans*, the causative agent of leptospirosis (McBride *et al*, 2005; Radolf, 1996; Tilly *et al*, 2007). The most distinctive feature of this group of bacteria is their spiral or wavelike morphology (Tilly *et al*, 2007). This spiral morphology is believed to confer increased speed and motility for the bacteria and allow for movement within more viscous environments (Motaleb *et al*, 2015; Yang *et al*, 2016). The bacteria within this family are also interesting because they are extremely invasive but contain little to no known toxins (Fraser *et al*, 1997; Hyde *et al*, 2011a). Based on this, it is believed that the pathogenesis is due to bacterial burden and the host immune response rather than bacterial toxicity (Fraser *et al*, 1997; Steere, 2001).

Borrelia burgdorferi is a bloodborne, microaerophilic, obligate parasite. They can range from 4 to 30um in length and .2 to .3 um in helices width (Johnson *et al*, 1984; Barbour, 1986). They are considered gram-negative-like spirochetes due to their similar dual-membrane system. However, they differ widely from true gram-negative bacteria because they do not contain lipopolysaccharides in their membrane (Takayama *et al*, 1987). Instead, they contain abundant lipoproteins (Fraser *et al*, 1997). Furthermore, they contain an endoflagella, as opposed to the typical external flagella, that resides in the periplasmic space and is attached to both ends of a protoplasmic cylinder. The flagella are composed of seven flagellar proteins that are wrapped around the protoplasmic cylinder, providing its unique spiral shape as well as its motility (Johnson, 1977; Barbour, 1986; Sultan *et al*, 2013). *B. burgdorferi* also exist solely within an enzootic cycle featuring *Ixodes* ticks as the vector and small vertebrates, typically mammals and birds, as hosts (Radolf *et al*, 2012).

The Borrelia genome consists of 1 linear chromosome and up to 21 linear and circular plasmids, typically with 12 linear and 9 circular. The linear chromosome is approximately 910 kb in size while the plasmids range from 5 to 56 kb (Fraser *et al*, 1997; Casjens *et al*, 2002). Only the linear chromosome and one circular plasmid, cp26, are essential for borrelial growth (Chaconas and Kobryn, 2010; Kobryn and Chaconas, 2002); however, the plasmids cp26, cp32, lp25, lp28-1, and lp54 have been shown to be essential within the enzootic cycle (Labandeira-Rey and Skare, 2001; Purser *et al*, 2003; Stewart *et al*, 2004a)(Figure 1.2). Because several of the plasmids are not essential for basic borrelial growth, *in vitro* propagation can lead to spontaneous loss of some plasmids, which can make genetic work difficult (Rosa *et al*, 2005). While the entirety of the *B. burgdorferi* genome has been sequenced, approximately 30% of the chromosome and much of the plasmids shared no significant homology with any previously identified genes (Fraser *et* al, 1997; Brisson *et al*, 2012), indicating areas of interest for future genetic work for *Borrelia*.

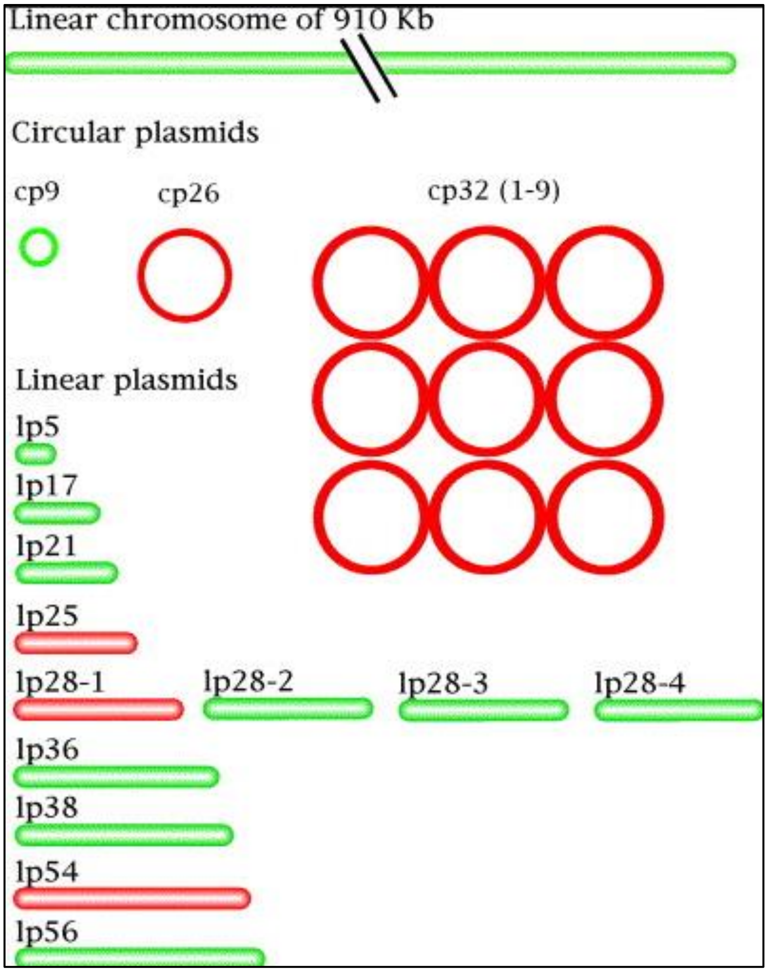
Linear chromosome of 910 Kb
Circular plasmids
cp9
cp26
cp32 (1-9)
Linear plasmids
lp5
lp17
lp21
lp25
lp28-1
lp28-2
lp28-3
lp28-4
lp36
lp38
lp54
lp56

Figure 1.2: *Borrelia burgdorferi* Strain B31 Genome.

All plasmids from the *B. burgdorferi* strain B31 genome. All plasmids essential for virulence are indicated in red. The remaining plasmids are unessential for virulence, though the chromosome and cp26 are essential for survival, and are indicated in green. Source: Stewart *et al*, 2004a.

Borrelia Morphology

Cell shape has been shown to contribute to bacterial pathogenesis. For instance, the curvature of *Caulobacter crescentus* was found to enhance colonization within aquatic environments with moderate flow in comparison to a rod-shaped version (Persat *et al*, 2014). Flagella are also important contributors to an organism's pathogenesis. Both the number and location of the flagella can affect the speed and the form of movement of a microbe, conferring a variety of potential advantages and disadvantages to its pathogenicity. For example, having multiple flagella may allow a pathogen to maneuver more quickly through its environment as opposed to a uniflagellar organism (Yang *et al*, 2016). Spiral shapes are believed to allow greater motility and speed for bacteria in more viscous environments (Motaleb *et al*, 2015; Yang *et al*, 2016), which would be ideal for bloodborne pathogens such as *B. burgdorferi.*

Since its discovery, many studies have attempted to understand the mechanisms responsible for the morphology of *B. burgdorferi*. Borrelia contains a bundle of 7 to 11 periplasmic flagella that are wrapped around the protoplasmic cylinder and attached at the two ends of the protoplasmic cylinder (Barbour and Hayes, 1986; Charon and Goldstein, 2002). Due to its unique placement in the cell, the borrelial flagella is responsible for both cell shape and cell motility (Motaleb *et al,* 2000). This tight connection between cell shape and motility can make it difficult to identify genetic factors responsible for specific morphological characteristics.

With advancement in genetic tools, parts of this morphological system have been elucidated. As of 2013, 24 genes had been identified associated with the flagella, chemotaxis, motility, or overall morphology gene regulation (Charon *et al*, 2012). FlaB, a major flagellar filament protein, and FlaA, a minor flagellar filament protein, are important contributors to the flagellar makeup. FlaB in particular created straight rod phenotypes when mutated and was non-motile (Charon and Goldstein, 2002; Charon *et al,* 2012; Ge *et al*, 1998; Motaleb *et al,* 2000). Other genes important for imparting spiral shape and motility to the organism were *flgE, fliF,* and *fliG2* (Charon and Goldstein, 2002; Li *et al*, 2010; Sal *et al*, 2008). A carbon storage regulator gene, *csrA,* is responsible for repressing FlaB and causes straight rod phenotype and elongation of cells when overexpressed (Sze *et al*, 2012).

B. burgdorferi also contain several copies of chemotaxis genes typically found in other bacteria, including 6 *mcp,* 2 *cheA, 3 cheY, 2 cheB, 2 cheR,* and 3 *cheW* genes (Charon *et al*, 2012; Fraser *et al*, 1997). Of these, the known borrelial chemotaxis pathway currently consists of MCPs, CheW3, CheA2, CheY3, and CheX. CheA2 phosphorylates CheY3, a key chemotaxis response regulator, to form CheY3-P. CheX, identified as essential for chemotaxis, is responsible for dephosphorylating CheY3-P (Charon *et al*, 2012; Motaleb *et al*, 2005; Motaleb *et al*, 2011). Two genes, *motA* and *motB*, are responsible for forming part of the motor complex and are both essential for motility in *B. burgdorferi* (Sultan *et al*, 2015).

A variety of other factors are involved in Borrelia morphology. Elongated cells can arise naturally when cells get old or when they are in nutritionally inadequate media (Barbour and Hayes, 1986). Several genes have been linked to a variety of other morphological phenotypes as well. *CsrA* mutants resulted in organisms that not only had flat-wave morphology but were elongated. The periplasmic flagella from these mutants were tightly bound to the protoplasmic cylinder and is a potential explanation for why longer cells tend to have flat-wave shape with small wavelength and less amplitude (Sze *et al*, 2011; Charon *et al*, 2012). *Hfq*, a global regulatory RNA-binding protein, and *DhhP*, a DHH-DHHA binding protein, have both been implicated as elongation-causing mutants (Lybecker *et al*, 2010; Ye *et al*, 2014).

While several plasmids have been noted as essential for virulence, only the chromosome and cp26 have been required for basic borrelial growth *in vitro*. Originally, only the *resT* gene was identified as essential for growth, as it was responsible for encoding the telomere resolvase gene (Byram *et al*, 2004). *Hfq* and *DhhP* have recently been shown to either significantly enhance borrelial growth or be essential for growth (Lybecker *et al*, 2010; Ye *et al*, 2014).

B. burgdorferi has been seen forming biofilm-like aggregates, typically well into stationary phase. Thus far, these aggregates have not been shown to confer any advantages or disadvantages in clinical consequences; however, there are speculations that these aggregates may enhance the binding of the pathogen to host tissues or may contribute to spirochetal successful transmission to the mammalian host and to ensuing disease (Barbour and Hayes, 1986; Dunham-Ems *et al*, 2009; Merilainen *et al*, 2015). This biofilm-like aggregation may also play an important role in neuroborreliosis (Di Domenico, 2018). Not much has been shown conclusively to explain the mechanisms or purpose behind these aggregates, but it is believed that the RpoN-RpoS-LuxS pathway is responsible for controlling aggregate formation. Mutations in all three of these genes led to the formation of smaller, looser aggregates than Wild-type (Di Domenico, 2018; Sapi, 2016). This pathway will be described in greater detail at a later point.

Enzootic Cycle

B. burgdorferi exists within an enzootic cycle consisting of *Ixodes* tick vectors and a variety of hosts, including small mammals, birds, and deer. There are several species responsible for transmission of *B. burgdorferi* and Lyme disease throughout the world; however, the main agent for transmission in the U.S. is *Ixodes scapularis,* the blacklegged or deer tick. Infection occurs predominantly in the Northeastern and Midwestern U.S. with 95% of infections occurring in 14 states consisting of Connecticut, Delaware, Maine, Maryland, Massachusetts, Minnesota, New Hampshire, New Jersey, New York, Pennsylvania, Rhode Island, Vermont, Virginia, and Wisconsin (Figure 1.1A, 1.1B). *Ixodes pacificus,* a species found on the Western coast of the US, has been found to transmit Lyme disease on rare occasions (only 1% rate of infection) (CDC, 2019).

The cycle for *Borrelia* features small mammals and birds as reservoir hosts, but large vertebrates such as domesticated pets and humans who become infected are considered accidental hosts as they typically prevent both the tick and the Borrelia from continuing through the cycle. Because Borrelia is not transmitted transovarially, larval ticks hatch from the eggs borrelia-free (Figure 1.3). During the late spring and early summer, the larval ticks have their first blood meal. If they feed on a reservoir host containing the bacteria, they become a vector. After this first blood meal, the larvae drop to the ground and molt into nymph forms. In the following spring, the nymph has a second bloodmeal. The typical hosts for this bloodmeal are small mammals and birds, creating a reservoir host that is unaffected by the bacteria. However, humans that get bitten by the infected tick get infected and become accidental hosts. After this bloodmeal, the nymphal tick drops to the ground and molts into an adult tick. In the fall, the adult tick seeks a deer to use as both a third bloodmeal and a breeding ground. After this bloodmeal, they drop to the ground, lay eggs, and the cycle begins again (Radolf, 2012) (Figure 1.3).

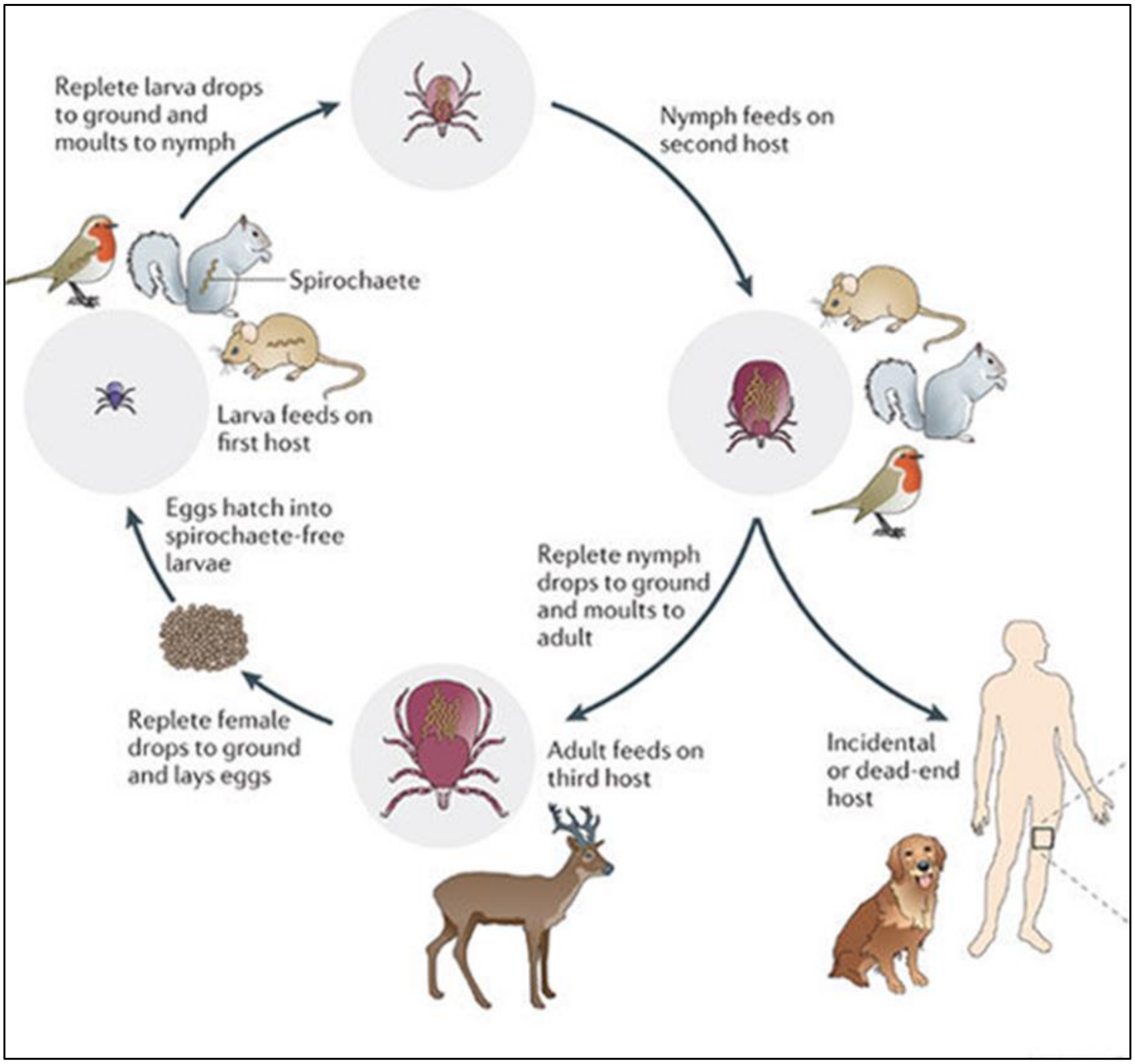
Replete larva drops
to ground and
moults to nymph
Nymph feeds on
second host
Spirochaete
Larva feeds on
first host
Eggs hatch into
spirochaete-free
larvae
Replete nymph
drops to ground
and moults to
adult
Replete female
drops to ground
and lays eggs
Adult feeds on
third host
Incidental
or dead-end
host

Figure 1.3 Enzootic Life Cycle of *B. burgdorferi* and *Ixodes* ticks

Ixodes tick larvae hatch spirochete-free and feed on first host. Feeding on a spirochete reservoir host results in the creation of a *Borrelia*-containing tick vector. After molting into nymph form, a second feeding occurs which creates more reservoir hosts or an infection in an accidental host. The ticks then molt into adults, feed on the third host, and breed.

Source: Radolf *et al*, 2012.

Lipoproteins and OspC

The outer surface lipoproteins that make up *B. burgdorferi* cellular membrane are essential for the organism to maintain normal, if any, functionality. There are 120 lipoprotein genes making up approximately 8% of the Borrelial genome (Fraser *et al*, 1997; Haake, 2000; Setubal *et al*, 2006). They have a large variety of functions, including stimulation of inflammation and the innate immune response, acting as protective immunogens, and binding to tick and host molecules for colonization and dissemination (Kenedy *et al*, 2012). These are abundant in the cell and are differentially expressed throughout the enzootic cycle and transmission of disease (Schwan *et al,* 1995; Schwan and Piesman, 2000).

Outer surface protein C (OspC) is a major lipoprotein expressed on the surface of Borrelia burgdorferi. It is differentially regulated throughout the borrelial life cycle and is inversely expressed with OspA. When the spirochetes are within the tick midgut prior to feeding, OspA is highly expressed and OspC is not expressed. Following a blood meal, OspA becomes downregulated and OspC becomes upregulated (Schwan *et al,* 1995). The difference in the expression of these two proteins led researchers to believe OspC is essential for transmission or establishment of infection. Researchers discovered that OspC is an antiphagocytic factor for the Borrelia. Without OspC, the bacteria were cleared and failed to establish infection (Carrasco *et al*, 2015; Grimm *et al*, 2004).

Alternative sigma factors allow for the regulation of different groups of genes within an organism. Two important alternative sigma factors typically associated with stress responses in bacteria, RpoS and RpoN, were found to be directly responsible for controlling OspC expression in *Borrelia burgdorferi* (Hubner, 2001). While RpoS typically acts as a stress response regulator in many bacteria, it does not in the case of *B. burgdorferi*. However, it does control the expression of key lipoproteins and virulence factors within the genome, including *ospC, dbpA,* and *luxS* (Caimano *et al,* 2004; Hubner *et al*, 2001; Sapi *et al*, 2016), allowing it to affect many aspects of the organism's infectivity and possibly morphology. In turn, RpoS expression is directly controlled by alternative sigma factor 54, or RpoN, both of which are required to establish infection in mammals (Fisher *et al*, 2005; Hubner *et al*, 2001; Smith *et al*, 2007) (Figure 1.4).

Various other proteins have been identified that help regulate this pathway. Borrelia oxidative stress response regulator (BosR) is a Zn-dependent transcriptional activator that activates *rpoS* transcription by binding to an upstream promoter site (Boylan *et al,* 2003; Hyde *et al*, 2009; Ouyang *et al*, 2009; Ouyang *et al*, 2011). It works in concert with response regulatory protein 2 (Rrp2), a σ^{54}-dependent transcriptional activator, to transcriptionally activate RpoS expression (Blevins *et al*, 2009; Boardman *et al*, 2008; Burtnick *et al*, 2007; Yang *et al*, 2003). Borrelia host adaptation regulator, BadR, is more highly expressed in conditions similar to the midgut of unfed ticks and become downregulated in conditions mimicking fed ticks. This protein was the first identified transcriptional repressor of the RpoN-RpoS pathway (Miller *et al*, 2013) (Figure 1.4). Mutations in the *BadR* gene were associated with failure to colonize in mice, growth defects in *in vitro* conditions, and increases levels of RpoS, BosR, OspC, and DbpA, indicating its potential role as a repressor of the RpoN-RpoS pathway (Miller *et al*, 2013).

Overall, the RpoN-RpoS pathway and OspC expression are regulated by external stimuli including temperature, CO2, cell density, pH, growth rate, and presence of blood, nutrients, metals, host signals. Lower temperatures, higher pH, and lower cell densities are associated with the midgut of an unfed tick, at which point the RpoN-RpoS pathway and the associated virulence factors are downregulated. As these external stimuli shift to match that of a fed tick, featuring higher temperature, lower pH, and increasing cell densities, the expression levels of the RpoN-RpoS pathway and its targets become elevated (Yang *et al*, 2002). Despite the increasing knowledge of the pathway controlling OspC expression, no genetic factors have been found that link these external stimuli with their expression-modifying effects.

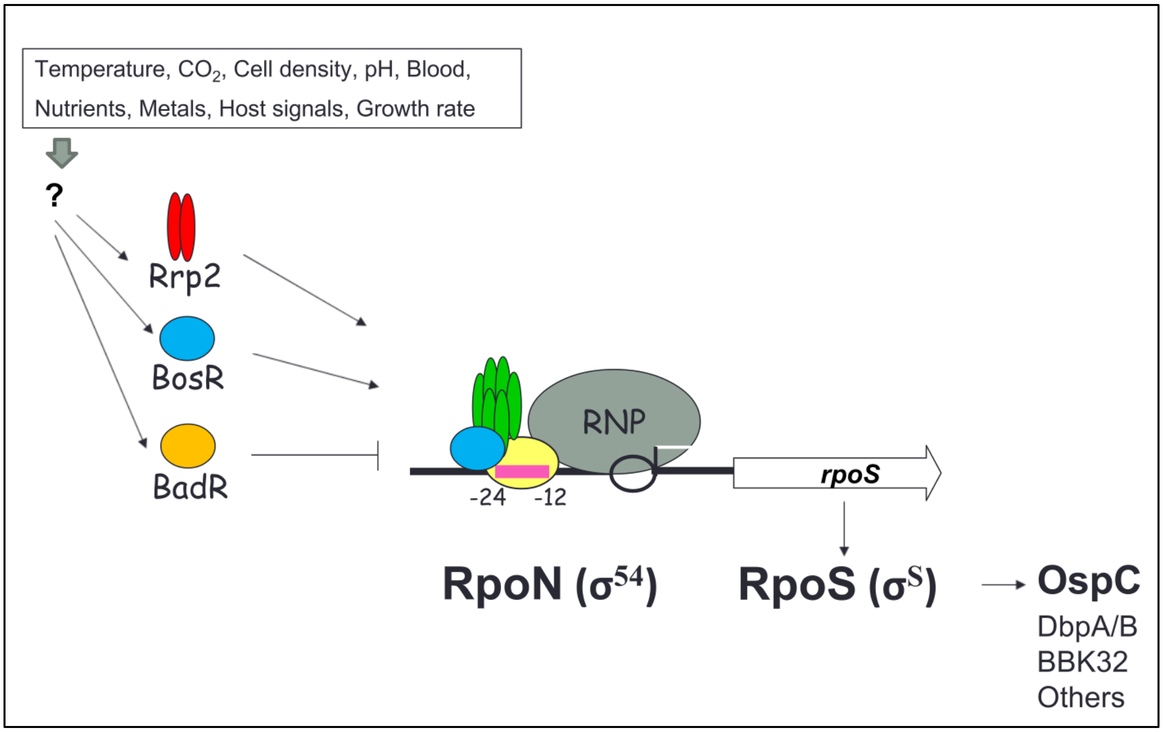
Temperature, CO_2, Cell density, pH, Blood,
Nutrients, Metals, Host signals, Growth rate
?
Rrp2
BosR
BadR
RNP
-24
-12
rpoS
RpoN (σ^{54})
RpoS (σ^{S})
OspC
DbpA/B
BBK32
Others

Figure 1.4: RpoN-RpoS Pathway Controlling OspC Expression

The RpoN-RpoS pathway is directly responsible for controlling levels of OspC. Expression levels are controlled by RpoS, which in turn is directly activated by RpoN. This pathway has two known activators, BosR and Rrp2, and one known repressor, BadR. There is currently no known factor connecting the environmental stimuli with this pathway.

Source: Dr. Frank Yang

Transposon Mutagenesis and the Mutant Library

Novel genetic tools have allowed researchers to delve deeper into genomic and proteomic studies of Borrelia. Transposon mutagenesis was used to create a mutant library of *Borrelia burgdorferi* in order to perform screening analyses. Strain B31 contains restriction and modification enzymes on plasmids lp25 and lp56, causing reduced transformation efficiency. These plasmids are still required for infectivity so strain 5A18NP1 was engineered to contain these plasmids while lacking the restriction/modification enzymes, allowing for higher transformation efficiency (Stewart and Rosa, 2008).

Cultures of this *B. burgdorferi* strain underwent transformation with an engineered plasmid called pGKT. This pGKT plasmid contains a mariner-based transposase gene, *himar1*, followed by a Kanamycin resistance marker (Figure 1.5B). These two genes are located outside of the two inverted terminal repeats that demarcate the transposon sequence of the plasmid. Within this transposon sequence lies a Gentamycin-resistance marker, *aacC1*, and a high-copy origin of replication, ColE1 (Figure 1.5B). At this stage, the transposase will work to insert the plasmid into the borrelial genome at a random site. Upon transposition into the genome, *himar1* and *kan* become spliced out while conferring Gentamycin resistance and the high-copy origin of replication, ColE1. This plasmid design allows for a single transposon mutagenesis to occur randomly within the borrelia genome (Stewart *et al,* 2004; Stewart and Rosa, 2008). Using this method, a library of *B. burgdorferi* mutants could be created and used for further genetic analysis.

Using a limiting dilution, calculated to obtain approximately 1 mutant per well, the samples were aliquoted into 96-well plates and grown in BSKII media. Over time, any wells contain successfully transformed and mutagenized borrelia should have changed from red to yellow. These samples were then taken and placed into another 96-well plate. The library consists of 72, 96-well plates.

Upon identification of a successful mutant transformant, the transposon sequence can be isolated from the mutant and transformed into *E. coli*, where ColE1 will enable the bacteria to express the gentamycin-resistance gene. Conferring gentamycin-resistance allows for antibiotic selection of both mutagenized borrelia sample and *E. coli* transformed with the transposon-containing plasmid. This plasmid can be isolated from the *E. coli* sample. Sequencing of the plasmid should consist of the transposon sequence as well as flanking regions from the borrelial genome, allowing identification of the transposon insertion site into the borrelial genome (Figure 1.5A) (Stewart *et al*, 2004; Stewart and Rosa, 2008).

A

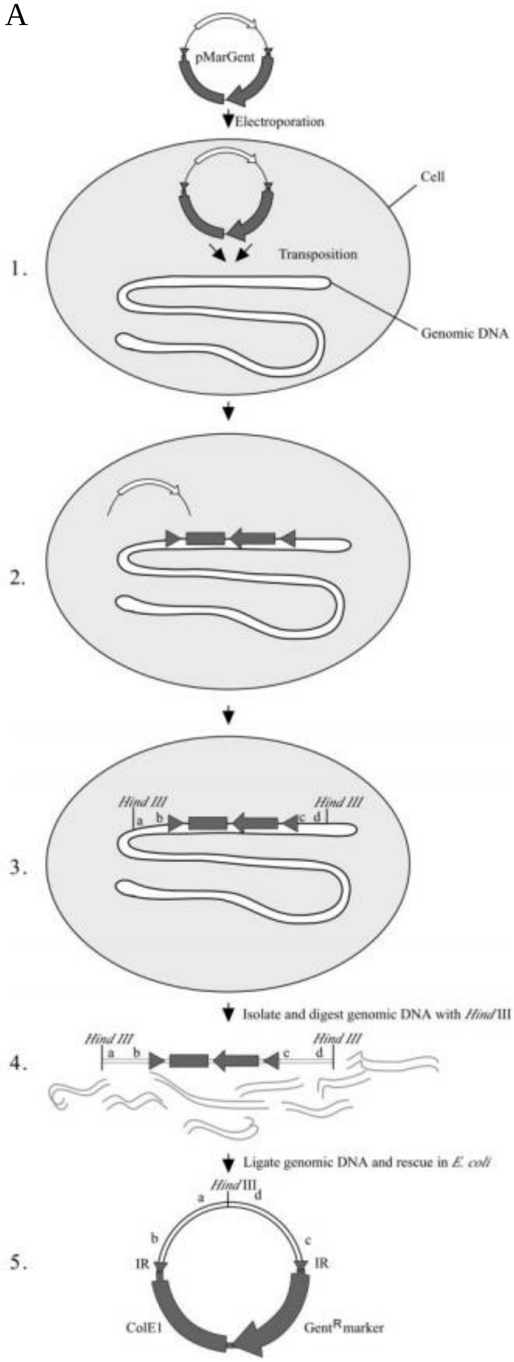

pMarGent
Electroporation
Cell
Transposition
1.
Genomic DNA
2.
Hind III
a
b
c
d
Hind III
3.
Isolate and digest genomic DNA with HindIII
Hind III
a
b
c
d
Hind III
4.
Ligate genomic DNA and rescue in E. coli
HindIII
a
d
b
c
5.
IR
IR
ColE1
Gent^R marker

B

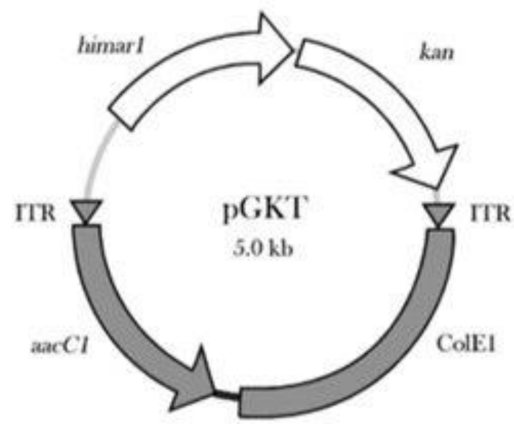

himar1
kan
ITR
pGKT
5.0 kb
ITR
aacC1
ColE1

Figure 1.5: Transposon Mutagenesis and the pGKT Plasmid

A, the engineered plasmid is transformed into *B. burgdorferi*. The transposon is inserted randomly into the genome while the transposase and *kan* genes are spliced out. DNA is extracted from the mutants of interest, digested with restriction enzyme, ligated to form plasmids. These are transformed into *E. coli* to be isolated and sequenced. B, the pGKT plasmid engineered for creation of the mutant library. This plasmid is used in place of pMargent, shown in Figure 1.5A.

Source: Stewart *et al*, 2004; Stewart and Rosa, 2008

Research Goals

Using the extensive mutant library created by former lab members, our lab seeks to execute two different research goals. The first is to identify novel genes responsible for *B. burgdorferi* morphology. While some factors have been identified relating to the shape, movement, and aggregation of the borrelial spirochetes, there is much left to be understood. Furthermore, there is evidence that morphological characteristics of bacteria can contribute to the pathogenesis of an organism. Our aim is to observe and confirm morphological mutants within the mutant library and identify the genes responsible for the given phenotype. The phenotypes that we can expect to see are elongated, decrease/lack of spiral, altered motility, enhanced aggregation, slow-growing, or any combination of those listed. In our search for novel morphology-related genes, it is likely that previously identified genes will arise in this screening process. These genes include those described previously: *flaB, flaA*, *flgE*, *fliF, fliG2,* and *csrA* for defective spiral mutants; *mcp, cheW, cheA, cheY, cheX, motA,* and *motB* for motility mutants; *csrA*, *hfq*, and *DhhP* for elongated mutants; and *rpoN, rpoS,* and *luxS* for aggregate mutants.

The second goal is to identify novel genes associated with the control of OspC expression. OspC has been identified as an antiphagocytic factor that is essential for establishing Lyme disease infection in mammals. It is in our interest to find and understand the mechanisms involved in regulating this protein. As discussed previously, the RpoN-RpoS regulatory pathway is directly responsible for OspC expression levels (Figure 1.4). Additional regulators, such as *BadR*, *BosR,* and *rrp2,* have been found to activate or repress this pathway. However, no links have been found between this pathway and the environmental stimuli that affect it. We hope to find not only novel

RpoN-RpoS-associated factors but genetic factors responsible for linking the external stimuli, such as temperature and pH, to this expression pathway.

MATERIALS AND METHODS

Bacterial Strains and Culture Conditions

Strain 5A18NP1 was engineered to lack restriction/modification enzymes found in B31. 5A18NP1 is the parent strain of the mutant library and is used as the Wild-type (Wt) sample in all experiments. BSK-II media from Barbour *et al* (1984) was used to culture *B. burgdorferi*. Cultures were made with or without Gentamycin and Kanamycin and at pH 7 or pH7.5, depending on purpose. All cultures were incubated at 37°C. Samples for morphology screening were grown for approximately 3 days in 1.8 mL of pH 7.5 BSKII with no antibiotics. After morphology checks, half of each sample was saved to make backstock. The remaining half was combined in 1:1 ratio with fresh BSKII (pH 7, with Gen and Kan) and grown for 5-7 days or until stationary phase. All stock samples of *B. burgdorferi* were stored in 15% BSKII-glycerol. DH5α competent cells were used for *E. coli* transformation. *E. coli* cultures were grown in LB media or on selective LB agar plates.

Morphology Screening

Dark field microscopy was used to observe borrelial phenotypes. All microscopy observations and imaging were performed at 40x using Olympus™ BX43 and Olympus™ CX41 microscopes. 6.8uL of sample was placed on glass microscope slide. Infinity Analyze™ was used to obtain and analyze images. Cell concentrations were determined by counting cells in field and multiplying by a constant of $3x10^5$. Possible morphology results include elongated mutants, defective/lost spiral, decreased motility, increased motility, aggregates, and slow-growing mutants.

OspC Screening

The samples from the morphology screenings were grown for 5-7 days until the samples reached stationary phase. At this point they were harvested via centrifugation at 8000 x g for 10 minutes in a tabletop centrifuge. The supernatant was discarded, and the cell pellets were washed in 500 ul of 1x PBS buffer. The centrifugation and wash steps were repeated once. After final centrifugation, the PBS was removed, and the cell pellet was re-suspended in 50 ul of 1x SDS buffer. The samples were then boiled in 100°C water for 5 minutes. The boiled samples were spun down for 1 min to collect any condensation and to ensure full dissolution of the pellet.

SDSPAGEs were performed using precast 12% polyacrylamide gels. Samples were loaded at 12 ul each. 3ul of ladder was loaded. Gels were run at 15 mA per gel. Gels were removed from casing and stained with Coomassie blue stain for 15-60 minutes. Gels were removed from stain and placed in de-stain buffer for 2-14 hours. Gels imaged using an HP Scanjet 4890 scanner. Identified mutants were tested again under differential conditions: pH 7-high density, pH 7.5-high density, and pH 7.5-low density.

Growth Curves

Growth curves were created by reviving samples in BSKII media. Upon reaching a desirable cell concentration, they were re-inoculated into 1.8mL of media at a starting concentration of $1x10^4$ cells/ml. Samples were observed every day. Resulting counts are the averages of 10 fields of view. Statistical analysis was performed using GraphPad Prism 8.0™.

SDS-PAGEs

Samples were revived in 1.8 mL of pH 7.5 BSKII media. Once reaching a desirable concentration for re-inoculation, Borrelial samples were re-inoculated at a 1:1 ratio into pH 7 BSKII media containing Gentamycin and Kanamycin. Samples were grown well into stationary phase to induce OspC expression. Pellets were harvested by centrifugation at 8000 x g for 10 minutes and washed twice with 500 uL of 1x PBS buffer. Washed pellets were re-suspended in 50 uL of 1x SDS buffer and placed in 100C water for 5 minutes. Samples identified as potential OspC mutants followed this same procedure except they were re-inoculated under 3 different conditions: pH 7.5 high concentration, pH 7.5 low concentration, and pH 7.5 high concentration.

12 uL samples for SDS-PAGEs were loaded into precast gels (Bio-Rad, 12%, 15-well) and run at 15mA/well for approximately an hour. Gels for SDS-PAGE were removed from cassette and stained with 1x SDS stain for 15 minutes. Then SDS stain was removed and the gels were placed in de-stain buffer for approximately 2-4 hours. Images were obtained using desktop scanner.

Cloning

Identified mutant samples were revived in 1.8 mL of BSKII media. Upon reaching appropriate concentration for re-inoculation, 1 mL of sample was inoculated into 40 mL of BSKII containing Gentamycin and Kanamycin. Samples were grown for approximately 4-5 days, or until sample reaches mid to late log phase. Samples were harvested by centrifugation at 8000 x g for 10 minutes. Genomic DNA was extracted using Wizard Genomic DNA extraction kit (Promega). DNA concentrations were determined using nanodrop. Using the appropriate amount of gDNA, Genomic DNA was digested with HindIII-HF restriction enzyme at 37°C for 2.5 hours.

The digested product was purified using phenol-chloroform extraction. Digested fragments were ligated using T4 Ligase. The ligated product was transformed into competent DH5α E. coli cells and plated on selective LB plates containing Gentamycin. After overnight incubation, a colony is isolated and inoculated into 5 ml LB media and grown overnight. The E. coli was harvested via centrifugation and underwent miniprep using Thermo Fisher GeneJET Miniprep Kit™. The plasmid DNA is then sent for sequencing using *flg* and *col* primers.

Identification of Transposon Insertion Site

Flg and *col* reads contain sequences from the regions flanking the transposon insertion. Sequencing reads were analyzed using NCBI Blast and compared to identify the Tn insertion site. NCBI Blast was also used to identify the gene in which the Tn was inserted.

Statistical Methods

All statistical analyses were made using GraphPad Prism 8.0™. Unpaired t-tests were used on all length, aggregate, and growth curve mutants. All p-values for the identified mutants can be found in the Results section.

RESULTS

Morphology Screening

Former members of the lab performed multiple transposon mutagenesis procedures on *Borrelia burgdorferi* cultures and the resulting transformants were isolated and transferred to wells within 96-well plates. They formed a substantial mutant library consisting of 72 96-well plates. During the project described here, a total of 14 of these plates were screened resulting in approximately 1350 individual samples undergoing screening. From these, 85 samples have been noted as potential morphology mutants. 37 of these samples have been double-checked and have undergone the appropriate analyses to confirm their phenotype, while 48 remain unconfirmed (Table 3.1).

The potential morphology mutations are Elongated, Defective spiral, Decreased motility, Increased motility, Aggregate, or Slow-growing. Elongated mutants and aggregate mutants were identified visually and confirmed using t-tests (Figures 3.1 – 3.4). All length measurements and statistical values for elongated mutants are detailed in Table 3.2. All measurements and statistical values for aggregate mutants are detailed in Table 3.3. Figure 3.5 shows growth curve results of several potential slow-growing mutants. This initial test eliminated all but six of the tested samples as potential mutants. These samples were initially identified as either "slow-to-grow" mutants, indicating a mutant that initially grew slowly but increases in growth rate partway through the curve, or "failure to thrive" mutants, indicating mutants that grew much more slowly throughout the curve and/or failed to reach stationary phase. Through statistical analysis, we discovered that all the "slow-to-grow" mutants (1E10, 5C2, and 48G5) were only statistically different from wild-type on 1 or 2 of the twelve-day curve and none of which were at the beginning of the growth curve. Though the statistics marked a small difference, the phenotype was not strong enough for us to pursue further processing of these mutants. The remaining mutants (1B5, 48G9, and 52G10) had growth curves that clearly differed from the Wt and so were confirmed as slow-growing mutants (Figure 3.6).

Defective spiral mutants were defined as mutants whose spiral shape appeared reduced or lost. Many of the defective spiral morphologies were found in tandem with elongated phenotype and occasionally appeared in segments rather than throughout the organism. Images were obtained of these samples; however higher magnification is needed to perform adequate analysis on these samples (Figure 3.7).

Increased and decreased motility mutants are defined as mutants who appear to move or “twitch” at rates higher or lower than typical Wt mutants. Motility mutants have not yet undergone any quantitative analysis and thus are only identified on a visual basis. They are listed here only as a list of potential mutants. It should be noted that several samples have been identified as having combinations of mutant phenotypes. Thus, all mutants conveying any defective spiral or motility morphologies have not been fully confirmed, though their lengths and aggregate morphologies may have been.

Morphology	**Samples**	**Total**	**Samples confirmed**	**Total confirmed**	**Samples unconfirmed**	**Total unconfirmed**
Elongated	1A8, 1H12, 2D1, 2E7, 3B5, 3D10, 3E8, 3H2, 5D2, 5D4, 5F11, 7D8, 7D11, 7H11, 45F12, 45H11, 46F5, 46F10, 47B3, **48C1**, 52D9, **52H8**, 54E3, 54G1, 56E9, 62A6, 62B2, 62C4, 62G5, 62H4	30	1A8, 1H12, 2D1, 2E7, 3E8, 3H2, 5D2, 5D4, 5F11, 7D8, 7D11, 7H11, 46F5, 47B3, 48C1, 52H8, 56E9	17	3B5, 3D10, 45F12, 45H11, 46F10, 52D9, 54E3, 54G1, 62A6, 62B2, 62C4, 62G5, 62H4	13
Defective Spiral	3E12, 28B8, 28E12, 62C7, 62C8	5	N/A	0	3E12, 28B8, 28E12, 62C7, 62C8	5
Decreased motility	3C6, 52A11	2	N/A	0	3C6, 52A11	2
Increased motility	1E12, 2B1, 3E9, 28C4, 45C7, 45H9, 47G11, 56F9, 62C5, 62F6	10	N/A	0	1E12, 2B1, 3E9, 28C4, 45C7, 45H9, 47G11, 56F9, 62C5, 62F6	10
Aggregate	1G4, 45B3, 47E11	3	1G4, 45B3, 47E11	3	N/A	0
Slow-growing	1E10, 5C2, 7B12, 47A9, 48H5, 54A1, 54A2	7	1E10, 5C2, 48H5	3	7B12, 47A9, 54A1, 54A2	4
Elongated and Defective spiral	2H1, 3B4, 3E5, 3F3, 3F10, 7F7, 7F10, 45D5, 45D7	9	2H1, 3F10, 45D5, 45D7	4	3B4, 3E5, 3F3, 7F7, 7F10	5
Elongated and Aggregate	**7A10**, 54G6, 54H10, 56A12, 56D12, 62A5, 62B6, 62C6	8	7A10, 62A5, 62C6	3	54G6, 54H10, 56A12, 56D12, 62B6	5
Elongated and Slow-growing	1B5, 2C1	2	1B5	1	2C1	1
Defective spiral	28C11, 62D5	2	N/A	0	28C11, 62D5	2

and Increased Motility						
Defective spiral and Decreased motility	48D4	1	N/A	0	48D4	1
Elongated, Defective Spiral, and Decreased Motility	5G11	1	5G11	1	N/A	0
Elongated, Defective Spiral, and Aggregate	56F5, **56H2**	2	56F5, 56H2	2	N/A	0
Elongated, Defective Spiral, and Slow-growing	5A7, 48G9, 52E10	3	5A7, 48G9, 52E10	3	N/A	0
TOTAL:		**85**		**37**		**48**

Table 3.1: Identified Morphology Mutants by Type

All potential morphology mutants categorized by type and marked as confirmed or unconfirmed. Samples that have undergone sequencing are listed in bold.

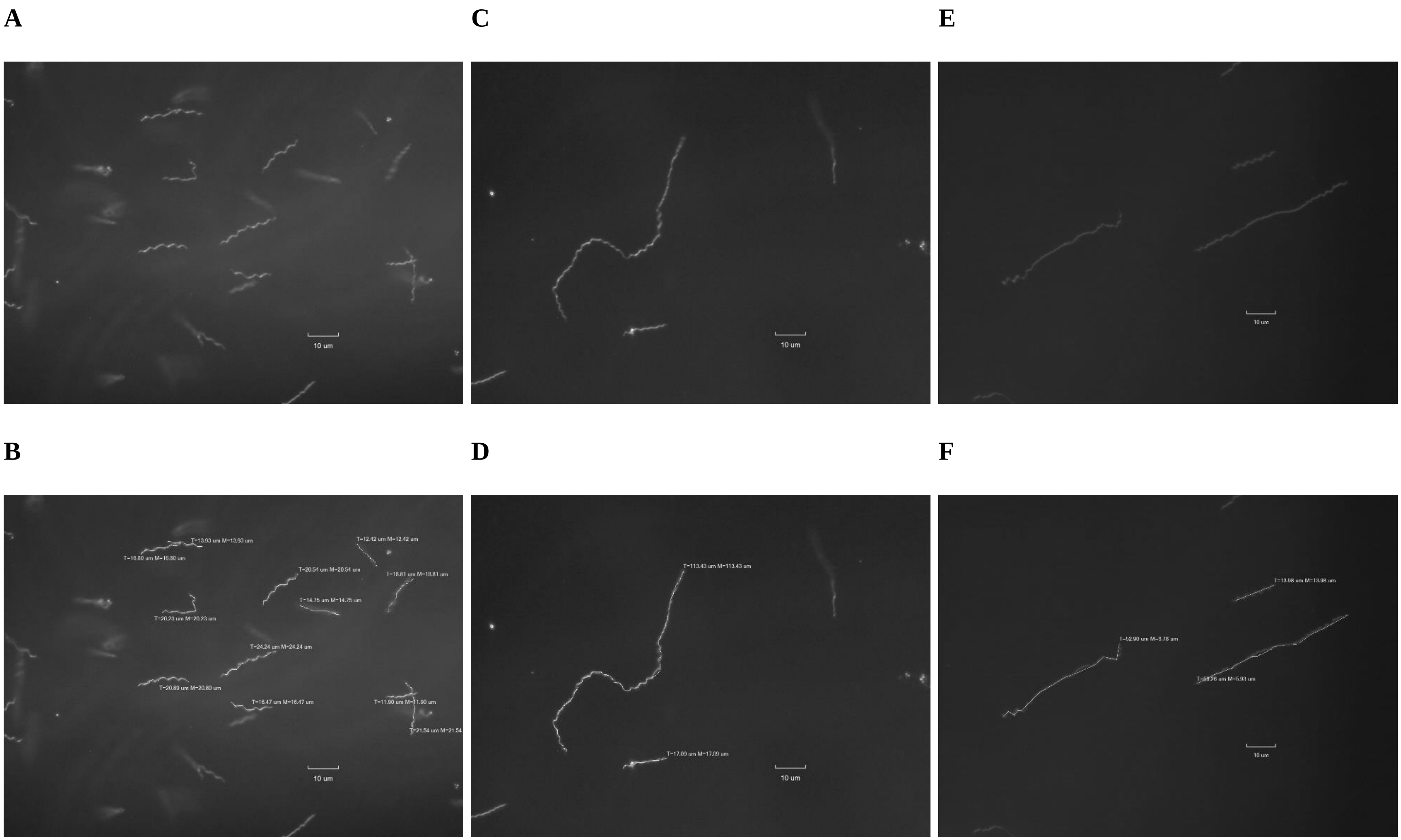
A
10 um
C
10 um
E
10 um
B
T=13.93 um M=13.93 um
T=16.80 um M=16.80 um
T=12.42 um M=12.42 um
T=20.54 um M=20.54 um
T=18.81 um M=18.81 um
T=14.75 um M=14.75 um
T=20.23 um M=20.23 um
T=24.24 um M=24.24 um
T=20.89 um M=20.89 um
T=16.47 um M=16.47 um
T=11.90 um M=11.90 um
T=21.54 um M=21.54
10 um
D
T=113.43 um M=113.43 um
T=17.09 um M=17.09 um
10 um
F
T=13.98 um M=13.98 um
T=52.90 um M=3.78 um
T=58.26 um M=5.93 um
10 um

Figure 3.1: Representative Images of Elongated Mutants

A and B, images of wild-type strain, 5A18NP1, with and without measurements. C and E, elongated mutants 1B5 and 46F10, without measurements. D and F, elongated mutants 1B5 and 46F10 with measurements.

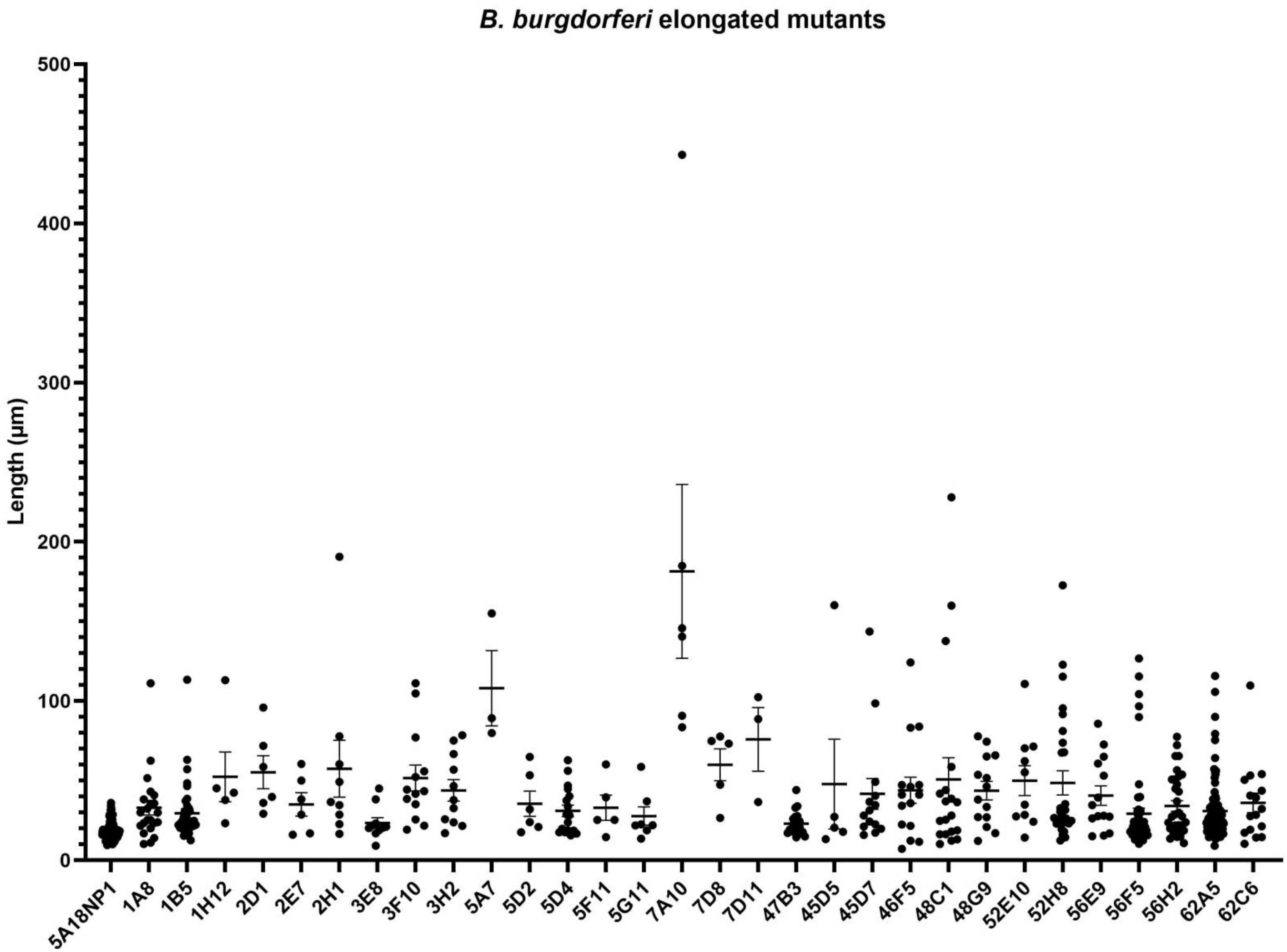
B. burgdorferi elongated mutants
Length (µm)
500
400
300
200
100
0
5A18NP1
1A8
1B5
1H12
2D1
2E7
2H1
3E8
3F10
3H2
5A7
5D2
5D4
5F11
5G11
7A10
7D8
7D11
47B3
45D5
45D7
46F5
48C1
48G9
52E10
52H8
56E9
56F5
56H2
62A5
62C6

Figure 3.2: *B. burgdorferi* Elongated Mutants

Dot plot representing the length measurements, means, and SDs of the Wt (5A18NP1) and identified elongated samples. All samples listed were compared with the Wt samples via t-test and had p-values lower than .05. All numerical data can be found in Appendix A.

Sample	Avg Length (µm)	n	p-value	*
Wt	18.16	94	N/A	N/A
1A8	33.01	22	<0.0001	****
1B5	29.50	38	<0.0001	****
1H12	52.40	5	<0.0001	****
2D1	55.26	6	<0.0001	****
2E7	35.07	6	<0.0001	****
2H1	57.49	9	<0.0001	****
3E8	23..47	10	.0100	*
3F10	51.63	13	<0.0001	****
3H2	43.87	11	<0.0001	****
5A7	108.1	3	<0.0001	****
5D2	35.47	6	<0.0001	****
5D4	31.03	17	<0.0001	****
5F11	32.99	5	<0.0001	****
5G11	27.76	7	.0003	***
7A10	181.4	6	<0.0001	****
7D8	59.96	5	<0.0001	****
7D11	75.89	3	<0.0001	****
47B3	22.98	20	.0011	**
45D5	47.82	5	<0.0001	****
45D7	41.69	14	<0.0001	****
46F5	43.99	15	<0.0001	****
48C1	50.83	19	<0.0001	****
48G9	43.66	14	<0.0001	****
52E10	49.95	10	<0.0001	****
52H8	48.57	28	<0.0001	****
56E9	40.61	14	<0.0001	****
56F5	29.29	56	<0.0001	****
56H2	35.08	33	<0.0001	****
62A5	30.83	89	<0.0001	****
62C6	36.05	16	<0.0001	****

Table 3.2: Measurements and P-values for Elongated Mutants

All elongated mutants were measured using Infinity Analyze™ and statistics analyses were performed using GraphPad Prism 8.0.

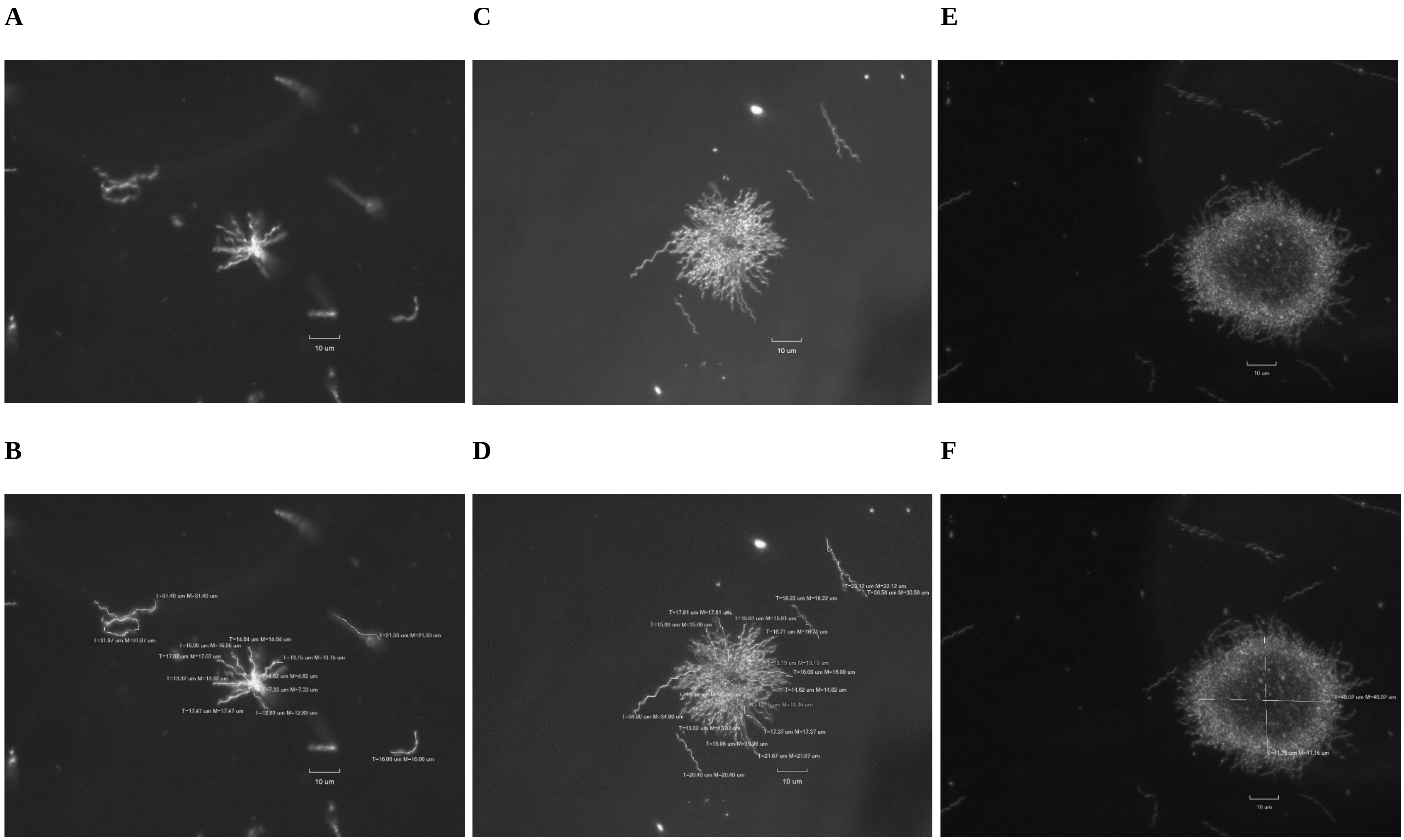
A
C
E
B
D
F
10 um

Figure 3.3: Representative Images of Aggregate Mutants

A and B, images of wild-type strain, 5a18NP1, with and without measurements. C and E, aggregate mutant strains 1G4 and 47E11 without measurements. D and F, aggregate mutant strains 1G4 and 47E11 with measurements.

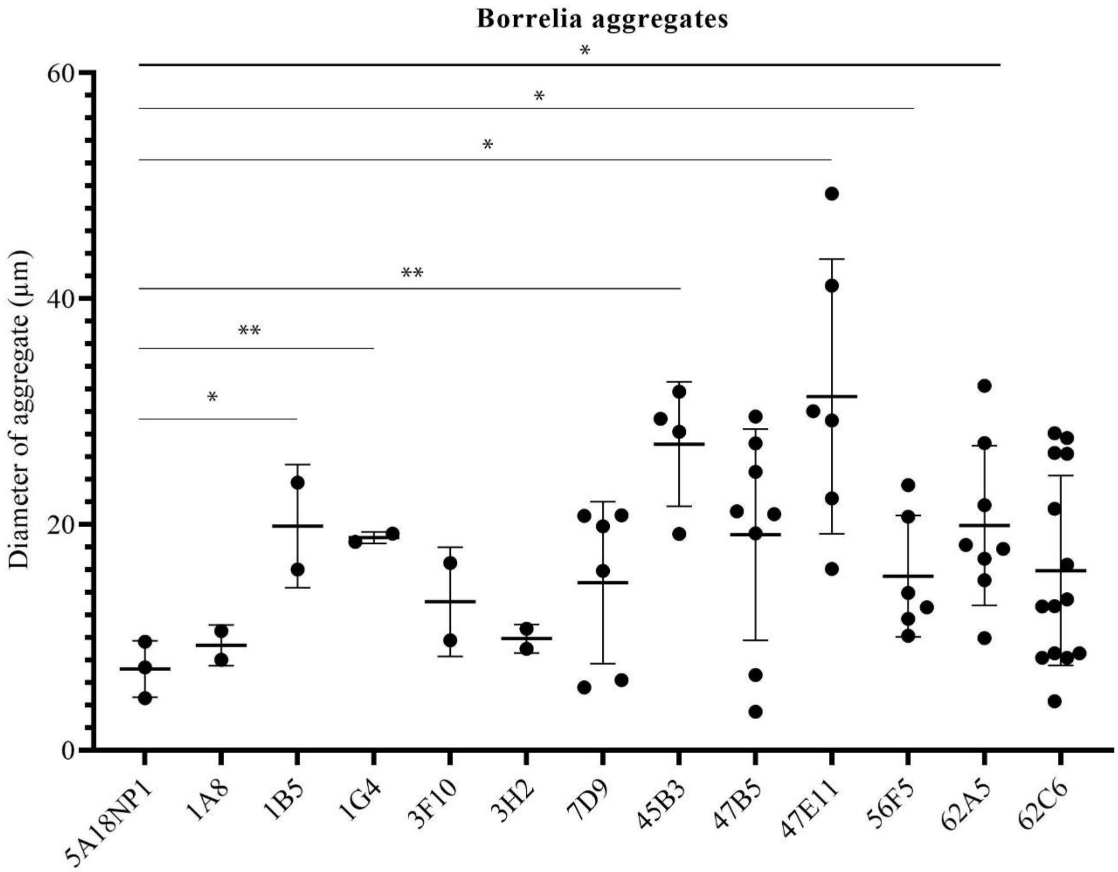
Borrelia aggregates
Diameter of aggregate (μm)
0
20
40
60
*
*
*
**
**
*
5A18NP1
1A8
1B5
1G4
3F10
3H2
7D9
45B3
47B5
47E11
56F5
62A5
62C6

Figure 3.4: *B. burgdorferi* Aggregate Mutants

Dot plot representing the measurements, means, and SDs of the diameters of the *Borrelial* aggregates. All samples listed were compared with Wt (5A18NP1) via t-test. Not all samples had p-values lower than .05. Samples considered significant are marked with * and **. All numerical data can be found in Appendix A.

Sample	Diameter (um)	n	P-value	*
Wt	7.19	3	N/A	N/A
1A8	9.28	2	.3914	N/A
1B5	19.86	2	.0342	*
1G4	18.83	2	.0086	**
3F10	13.16	2	.1557	N/A
3H2	9.88	2	.2684	N/A
7D9	14.84	6	.1250	N/A
45B3	27.12	4	.0023	**
47B5	19.10	8	.0643	N/A
47E11	31.34	6	.0133	*
56F5	15.43	6	.0436	*
62A5	19.90	8	.0158	*
62C6	15.92	14	.1021	N/A

Table 3.3: Measurements and P-values of Aggregate Mutants

All aggregate mutants were measured using Infinity Analyze™ and statistics analyses were performed using GraphPad Prism 8.0.

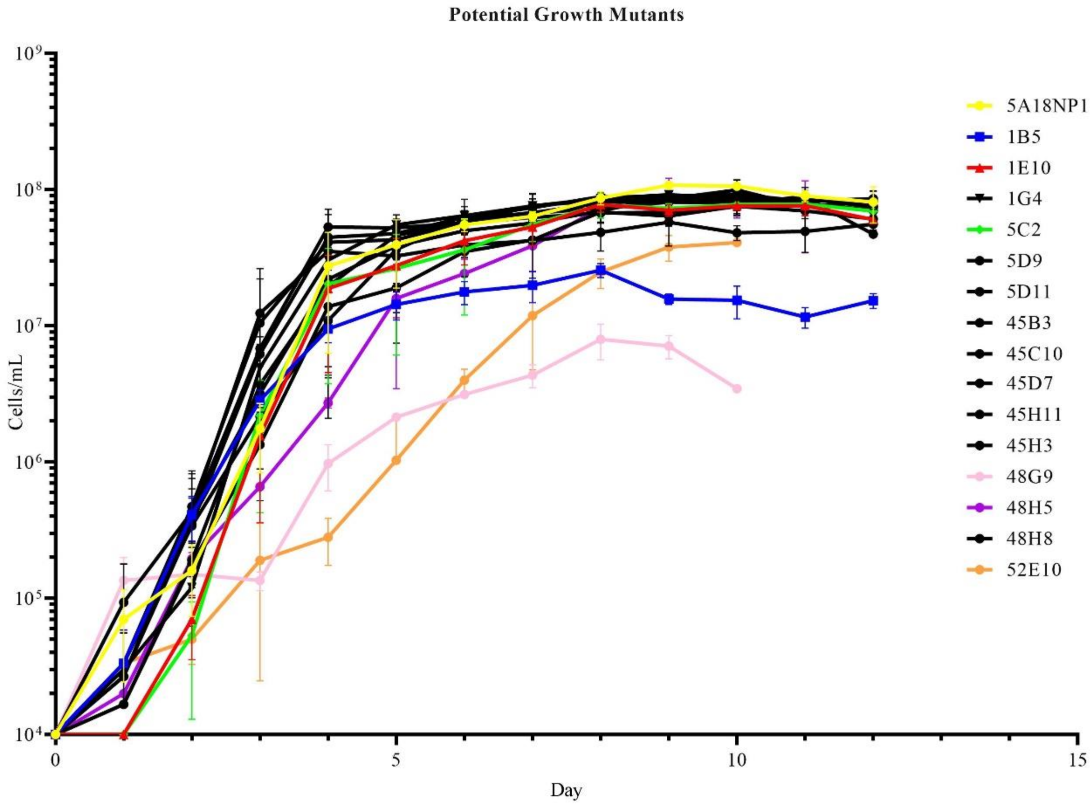
Potential Growth Mutants
Cells/mL
Day
10⁹
10⁸
10⁷
10⁶
10⁵
10⁴
0
5
10
15
5A18NP1
1B5
1E10
1G4
5C2
5D9
5D11
45B3
45C10
45D7
45H11
45H3
48G9
48H5
48H8
52E10

.

Figure 3.5: Potential *B. burgdorferi* Growth Mutants

Growth curve data of all samples originally identified as slow-growing mutants. Not all samples tested presented mutant phenotype. Slow-growing mutants identified from this experiment are represented in individual growth curves in Figure 3.4.

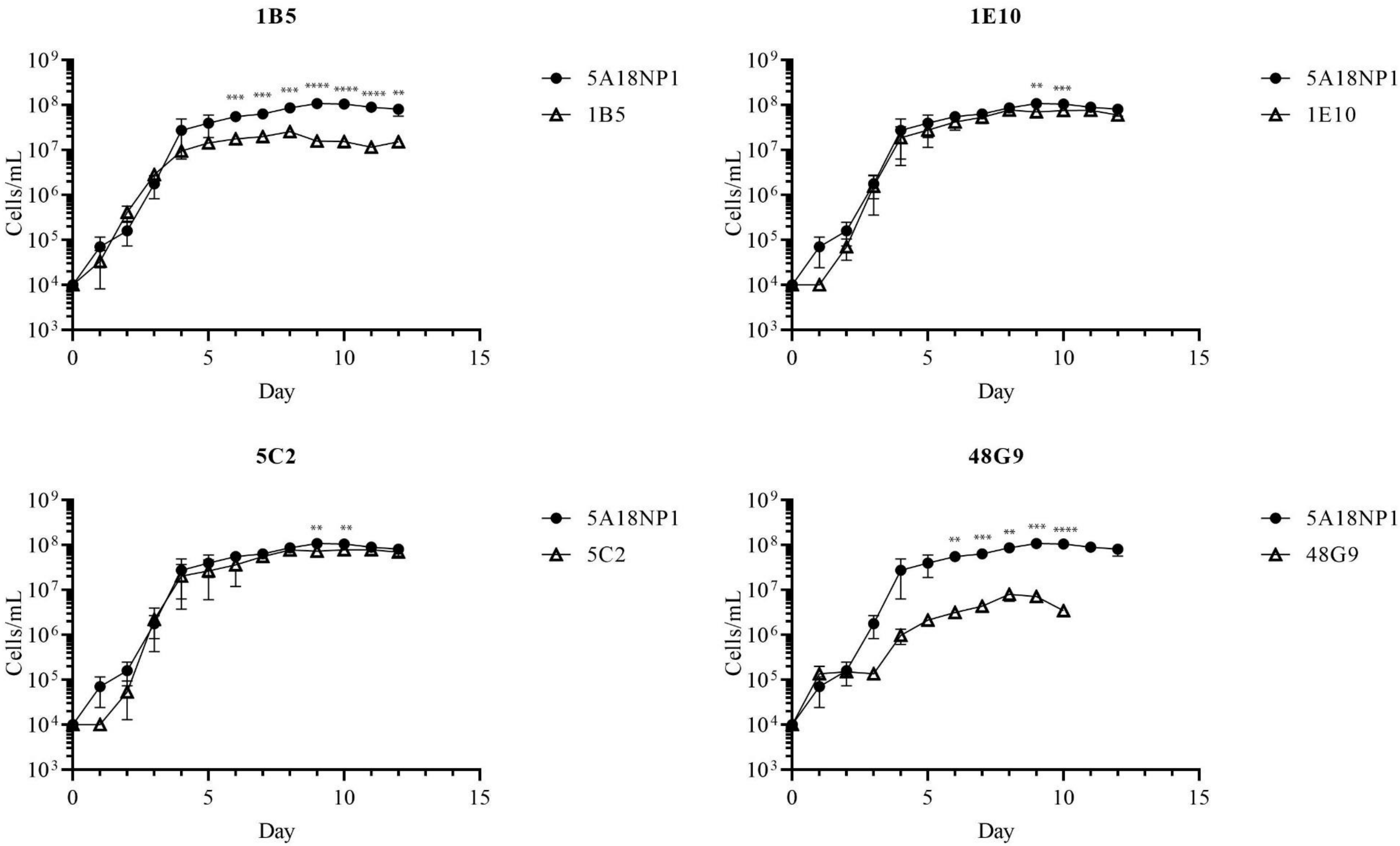
1B5
1E10
5C2
48G9
Cells/mL
Day
5A18NP1
1B5
1E10
5C2
48G9

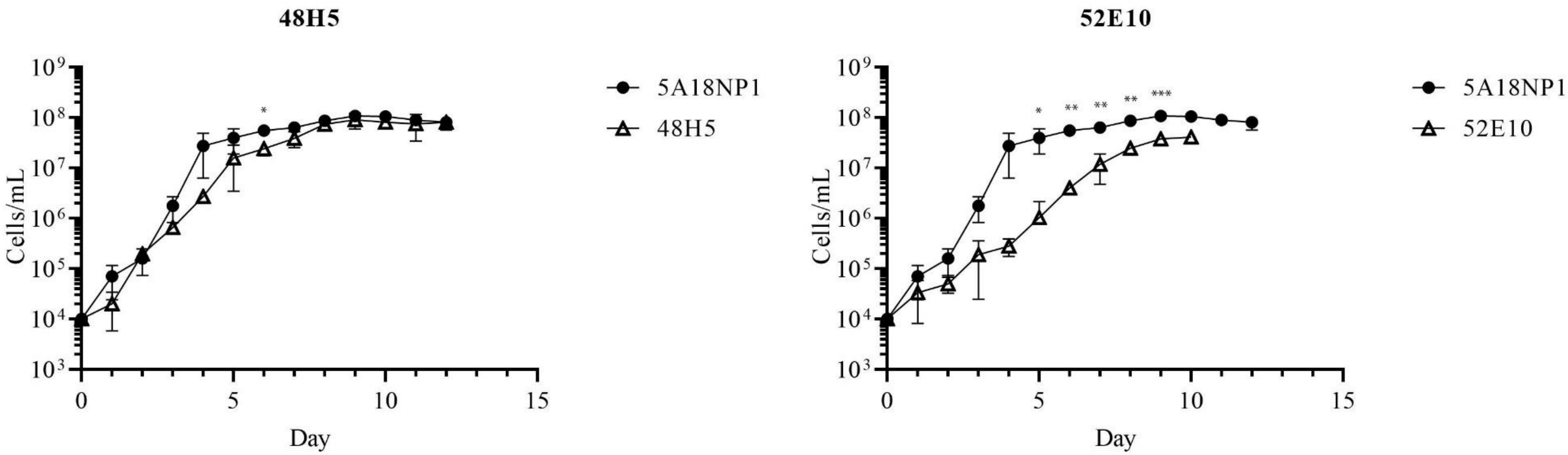
48H5
52E10
Cells/mL
Day
5A18NP1
48H5
52E10
10^3
10^4
10^5
10^6
10^7
10^8
10^9
0
5
10
15

Figure 3.6: Individual Growth Curves of Slow-Growing Mutants

The growth curves of the possible slow-growing mutants were isolated from the curves in Figure 3.3. From these we identified which samples showed strong slow-growing phenotype. Samples 1B5, 48G9, and 52E10 differ significantly from the Wt curve and is the most noticeable during the mid- to late-stages of the curve. 1E10, 5C2, and 48H5, however, are only noted to be statistically different on Days 9 and 10, which does not match our proposed "slow-to-grow" phenotype.

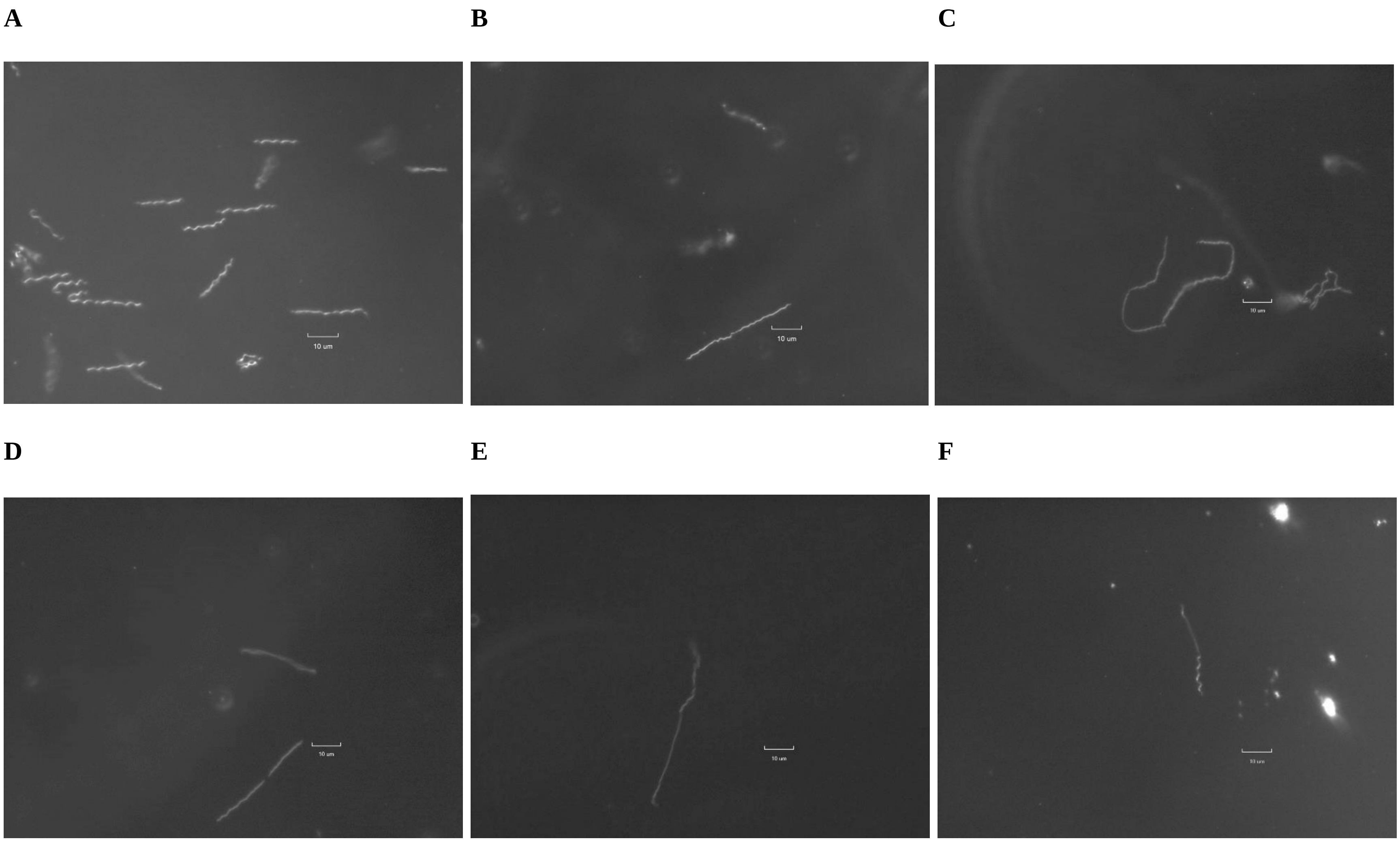
A
B
C
D
E
F
10 um
10 um

Figure 3.7: Representative Images of Defective Spiral Mutants

A, Image of wild-strain, 5A18NP1. B-F, images of potential defective spiral mutants 2E7, 7F7, 45D5, 48G9, and 52E10, respectively.

OspC Screening

SDS-PAGEs were used to run preliminary screenings on all the mutant library samples. Figure 3.8 shows the SDS-PAGEs run on Plate 46 to represent the screenings run on all the mutant library plates. Only one OspC expression mutant, 46A2, was found from this plate and was marked as a complete OspC deficient mutant. From all of the screenings, 66 potential OspC expression mutants were found. Of these, 13 were identified as complete knockouts of OspC expression while 22 and 31 were identified as underexpressed and overexpressed, respectively (Table 3.4). Because the focus in this experiment has been on those samples completely lacking OspC expression, the underexpressed and overexpressed samples have not yet been confirmed. 8 of the 13 mutants proposed to be lacking OspC were re-grown and the SDSPAGES were repeated (Table 3.4; Figure 3.9). The samples 28C2, 28F7, 45C4, 46A2, 52G11, and 56H11 were confirmed complete OspC deficient mutants. 45B3 and 52G10 have also been confirmed as lacking OspC; however, they were not run in the procedure shown in Figure 3.9.

Of the confirmed OspC depleted mutants, 6 samples had undergone conditional SDS-PAGE in which they were grown in different pH's (7 and 7.5) and to different concentrations (low and high) in order to further affirm their mutant OspC expression (Figure 3.10). Due to the effects of differing pH and cell densities on OspC expression levels in Wt, three conditions are used to confirm OspC expression phenotype. Low cell-density and higher pH (7.5) is used somewhat like a negative control, high cell density with pH 7.5 matches standard culture conditions, and high cell density with lower pH (7) is used to enhance OspC expression. Samples 52G10, 52G11, and 56H11 were successfully tested under these conditions and showed clear depletion of OspC, while samples such as 52B7, 52F1, and 52F11 did not (Figure 3.10).

OspC Expression	**Samples**	**Total**	**Samples confirmed**	**Total confirmed**	**Samples unconfirmed**	**Total unconfirmed**
No expression	28C2, **28F7, 45B3, 45C4**, 45F5, **46A2, 52G10,** 52G11, 56H11, 62A2, 62B3, 62E3, 62H5	13	28C2, 28F7, 45B3, 45C4, 46A2, 52G10, 52G11, 56H11	8	45F5, 62A2, 62B3, 62E3, 62H5	5
Underexpression	1F5, 3F10, 45A5, 45B11, 45B12, 45C2, 45C8, 45C9, 45D1, 45E7, 45E9, 45E11, 45H4, 47A6, 47B5, 47D11, 47E5, 47F1, 47F6, 48H12, 56D1, 56G5	22	N/A	N/A	1F5, 3F10, 45A5, 45B11, 45B12, 45C2, 45C8, 45C9, 45D1, 45E7, 45E9, 45E11, 45H4, 47A6, 47B5, 47D11, 47E5, 47F1, 47F6, 48H12, 56D1, 56G5	22
Overexpression	1D12, 2A6, 2A9, 2A10, 2A12, 2B6, 2B11, 2B12, 2D12, 2G11, 2H7, 2H12, 3B2, 3D2, 3D3, 3F12, 3H3, 28A8, 28C4, 28G9, 45B2, 45C7, 45C10, 52D1, 52D12, 52E12, 52G7, 62B4, 62F3, 62F4, 62H1	31	N/A	N/A	1D12, 2A6, 2A9, 2A10, 2A12, 2B6, 2B11, 2B12, 2D12, 2G11, 2H7, 2H12, 3B2, 3D2, 3D3, 3F12, 3H3, 28A8, 28C4, 28G9, 45B2, 45C7, 45C10, 52D1, 52D12, 52E12, 52G7, 62B4, 62F3, 62F4, 62H1	31
Total		**66**		**8**		**58**

Table 3.4: List of OspC Expression Mutation Types and Identified Samples

All of the potential OspC mutants are listed according their mutation type. Confirmed mutants had undergone secondary SDSPAGE testing while unconfirmed mutants have not. Because the focus was on complete OspC knockouts, only these have undergone confirmatory testing thus far. Samples that have undergone sequencing are listed in bold.

Plate 46

lad Wt A1 A2 A3 A4 A5 A6 A7 A8 A9 A10 A11 A12 B1

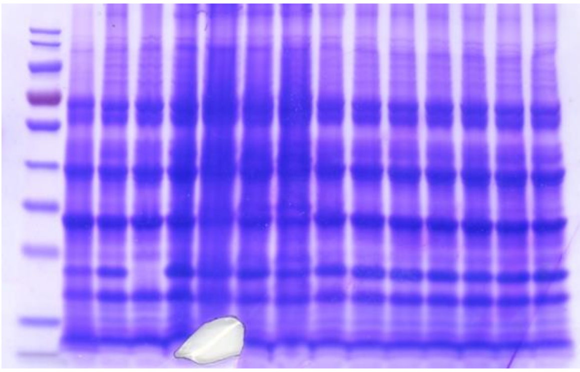

B2 lad B3 B4 B5 B6 B7 B8 B9 B10 B11 B12 C1 C2 C3

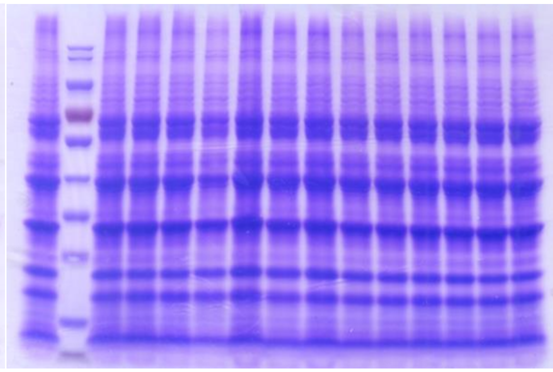

C4 C5 lad C6 C7 C8 C9 C10 C11 C12 D1 D2 D3 D4 D5

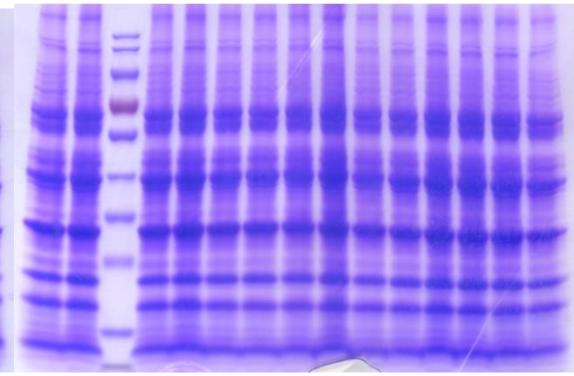

D6 D7 D8 lad D9 D10 D11 D12 E1 E2 E3 E4 E5 E6 E7

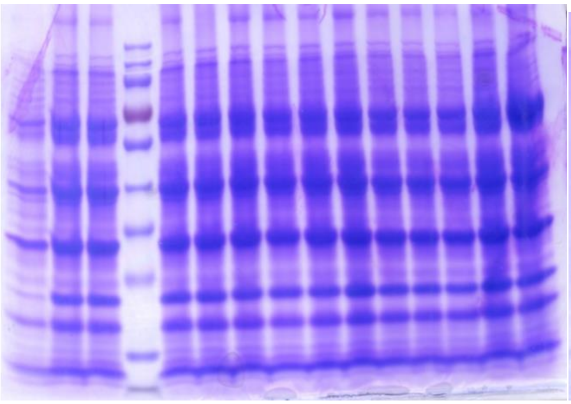

lad Wt E8 E10 E11 E12 F1 F2 F3 F4 F5 G6 G11 H5 H10

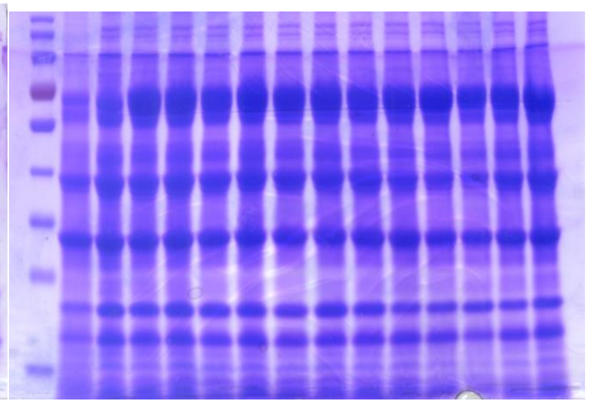

Figure 3.8: SDS-PAGEs of Plate 46 Samples

Preliminary OspC screening of samples from Plate 46 via SDS-PAGE. These are representative of the screenings performed on all of the samples within the OspC screening process.

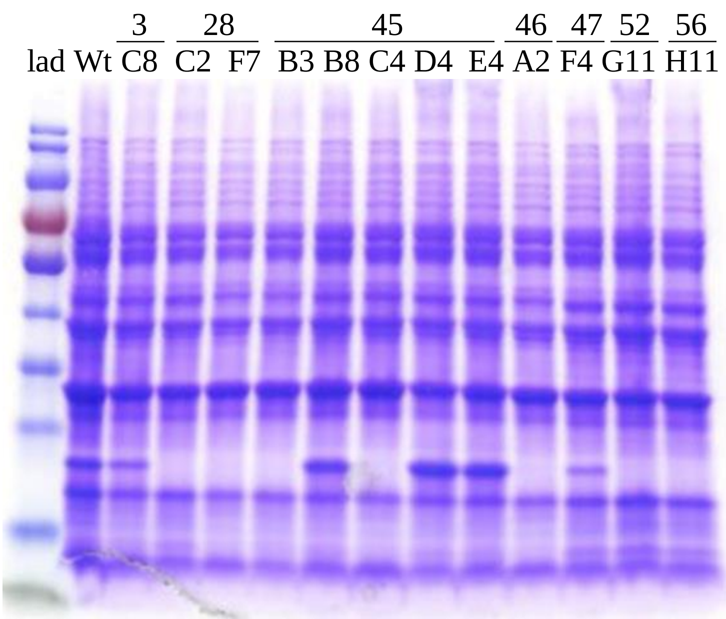
3
28
45
46
47
52
56
lad Wt C8 C2 F7 B3 B8 C4 D4 E4 A2 F4 G11 H11

Figure 3.9: SDS-PAGE of Potential OspC Deficient Mutants

The potential OspC mutants were regrown and used in a second SDS-PAGE to verify OspC-lacking phenotype. Samples 3C8, 45B8, 45D4, 45E4, and 47F4 identified as false mutants, however 47F4 may be underexpressed. The remaining samples were confidently labeled as OspC deficient mutants.

	Lad	5A18NP1			52B7			52F1			52F11		
pH		7	7.5	7.5	7	7.5	7.5	7	7.5	7.5	7	7.5	7.5
Conc.		H	L	H	H	L	H	H	L	H	H	L	H

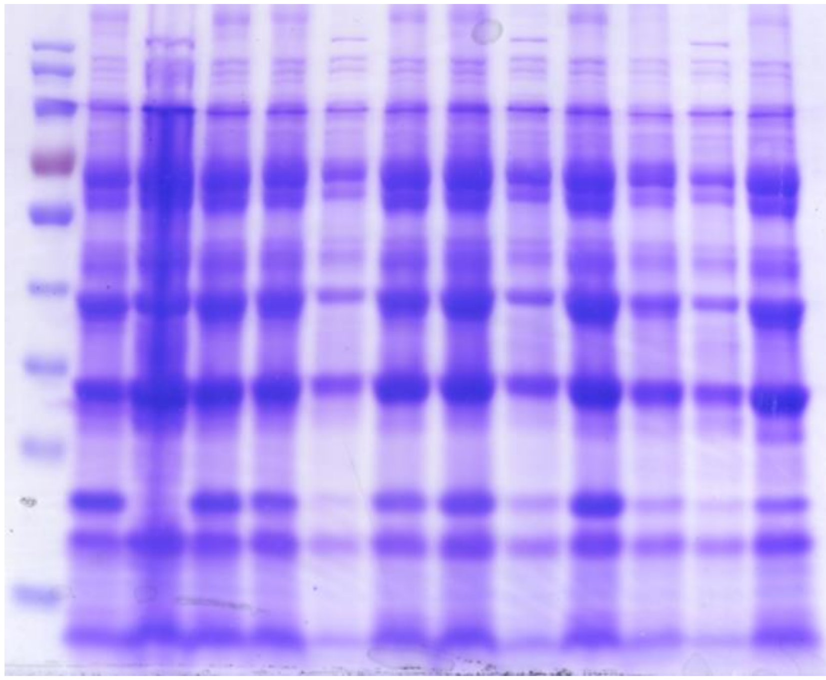

	5A18NP1			52G10			52G11			56H11		
pH	7	7.5	7.5	7	7.5	7.5	7	7.5	7.5	7	7.5	7.5
Conc.	H	L	H	H	L	H	H	L	H	H	L	H

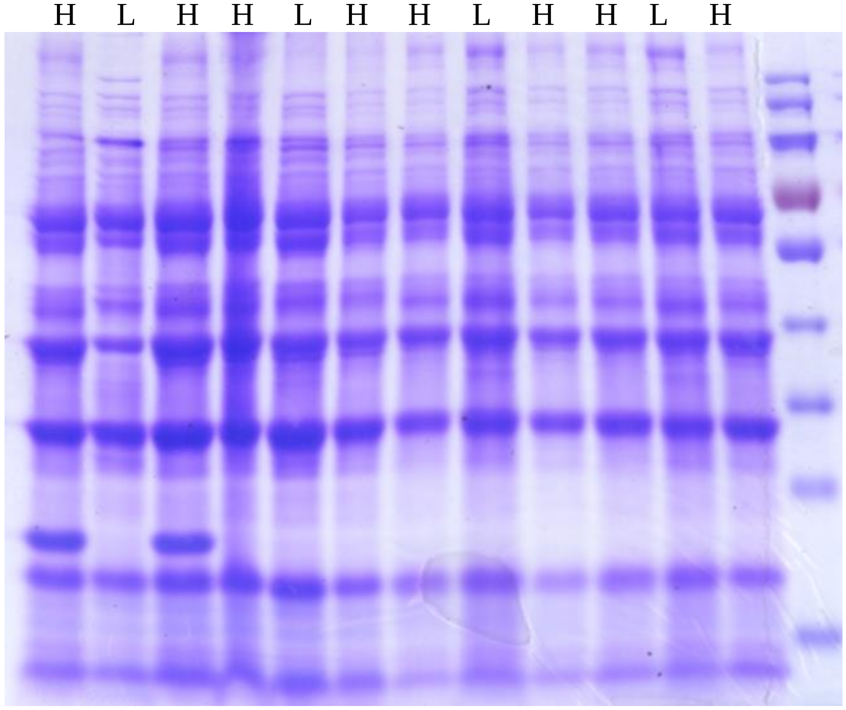

Figure 3.10: Conditional SDS-PAGEs of Potential OspC-Lacking Mutants

Samples were checked under three different conditions. Low-density, pH 7.5 samples act as negative controls because they are sub-optimal for OspC expression. High-density, pH 7 samples are the most optimal for OspC expression and thus act as a positive control. High-density, pH 7.5 samples are representative of conditions similar to *in vivo* conditions. Samples 52B7, 52F1, and 52F11 were found to be false mutants while 52G10, 52G11, and 56H11 were confirmed.

Sequencing and Identification of Tn Insertion Site

Identified and confirmed mutants from both screens underwent cloning in order to obtain the plasmid containing the transposon insertion site. The plasmids were transformed into DH5alpha competent cells and grown on selective plating to obtain isolated colonies. The plasmid was obtained from these colonies and sent out for sequencing using Col and Flg primers. The insertion should have entered into one position in the genome, and the sequencing data points to the insertion site of the transposon sequence. Eleven samples, 4 morphology mutants and 7 OspC mutants, were successfully sequenced and identified (Table 3.5).

Most of the morphology mutants resulted in novel genes. 7A10, 48C1, and 56H2 had mutations in BB_0043, BB_0420, and BB_0811, respectively. All three of which were previously unstudied hypothetical proteins (Table 3.5, Figure 3.11 A-C). Further studies will need to be conducted to characterize these genes and their association with borrelial morphology. The mutated gene in 52H8 was surface-located membrane protein 1, LMP1 (Table 3.5, Figure 3.11D). Previous studies have identified this as a membrane protein required to resist or evade the host-adaptive immune response, but none of these studies compared morphologies or noted morphological mutants during their work (Kenedy *et al,* 2012; Koci *et al,* 2018; Yang *et al,* 2009; Yang *et al,* 2010).

Four of the seven OspC mutants contained mutations within the OspC gene itself (Table 3.5; Figure 3.11H). The remaining three OspC mutant samples resulted in unique genes, however. Mutations were found in fibronectin-binding protein gene *bbk32*, adenine deaminase gene *bbk17* or *adeC*, and ribonuclease HII gene *rnhB* (Table 3.5; Figure 3.11 E-G) resulting in depleted OspC expression. The BBK32 protein has already been extensively studied and identified a surface protein that is important for enhancing infectivity potential in *B. burgdorferi* and is regulated by the Rrp2-RpoN-RpoS pathway (He *et al,* 2007; Seshu *et al,* 2006). However, current studies have only suggested that it is co-regulated with OspC. None so far have studied whether BBK32 plays any role in controlling OspC levels.

Bbk17, or *adeC,* has also been shown to contribute to mammalian infectivity (Jewett *et al,* 2007). It encodes an adenine deaminase and is required for the direct deamination of adenine to hypoxanthine, a purine important for the salvage of adenine in many prokaryotic species (Jewett *et al*, 2007; Nygaard *et al*, 1996). Unlike BBK32, the mechanisms controlling AdeC levels have not yet been studied. The protein's affiliation with the RpoN-RpoS pathway and OspC regulation remain to be seen. The product of the third gene, *rnhB*, was determined based off of sequence homology (Fraser *et al*, 1997), but no further studies have been conducted to characterize the gene or its protein product.

Sample ID	**Phenotype**	**Confirmation**	**Gene ID**	**Gene Name**	**Gene Product**	**Insertion Site**
7A10	Elongated, aggregate	Via imaging and statistical analysis	BB_0043	unnamed	Unknown, predicted protein coding gene	42392, 42393
48C1	Elongated	Via imaging and statistical analysis	BB_0420	unnamed	Sensory transduction histidine kinase, putative	433448, 433449
52H8	Elongated	Via imaging and statistical analysis	BB_0210	LMP1	Surface-located membrane protein 1	212916, 212917
56H2	Elongated, defective spiral, aggregate	Via imaging and statistical analysis	BB_0811	unnamed	Conserved hypothetical protein	858615, 858616
28F7	Complete OspC deficiency	Via repeated SDS-PAGE	BB_K32	bbk32	Fibronectin-binding protein	21036, 21037
45B3	Complete OspC deficiency	Via repeated SDS-PAGE	BB_B19	OspC	Outer surface protein C	17213, 17214
45C4	Complete OspC deficiency	Via repeated SDS-PAGE	BB_K17	bbk17	Adenine deaminase C	11791, 11792
46A2	Complete OspC deficiency	Via repeated SDS-PAGE	BB_0046	rnhB	Ribonuclease HII	45787, 45788
52G10	Complete OspC deficiency	Via repeated SDS-PAGE	BB_B19	OspC	Outer surface protein C	16946, 16947
52G11	Complete OspC	Via repeated SDS-	BB_B19	OspC	Outer surface protein C	16946,

	deficiency	PAGE				16947
56H11	Complete OspC deficiency	Via repeated SDS-PAGE	BB_B19	OspC	Outer surface protein C	16946, 16947

Table 3.5: List of Sequenced Samples and their Transposon Insertion Sites

All samples to be successfully cloned and sequenced, with morphology mutants listed first followed by OspC mutants. Imaging and statistical analysis can be found in the Morphology Screening section. SDS-PAGEs can be found in the OspC screening section. Gene ID refers to the original name/location of the gene according to the sequencing performed in strain B31.

A

7A10 – Elongated, Aggregate

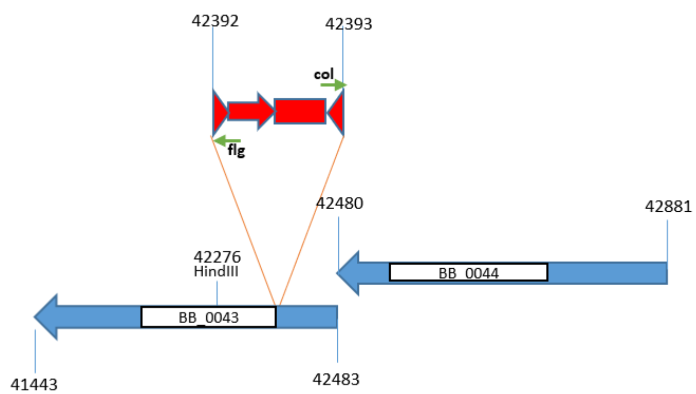

Tn insertion between 42392-42393

Gene: BB_0043

Gene product: unknown, predicted protein coding gene

B

48C1 – Elongated

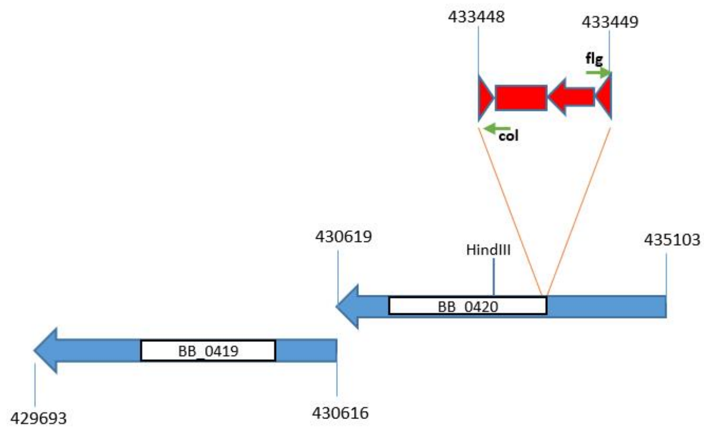

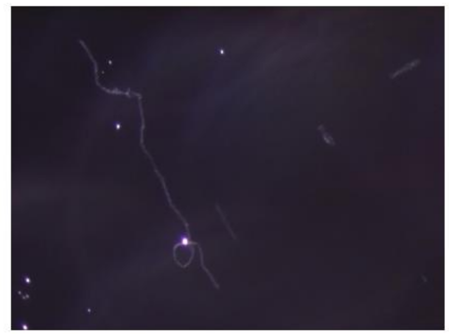

Tn insertion between 433448 and 433449

Gene: BB_0420

Gene product: sensory transduction histidine kinase, putative

C

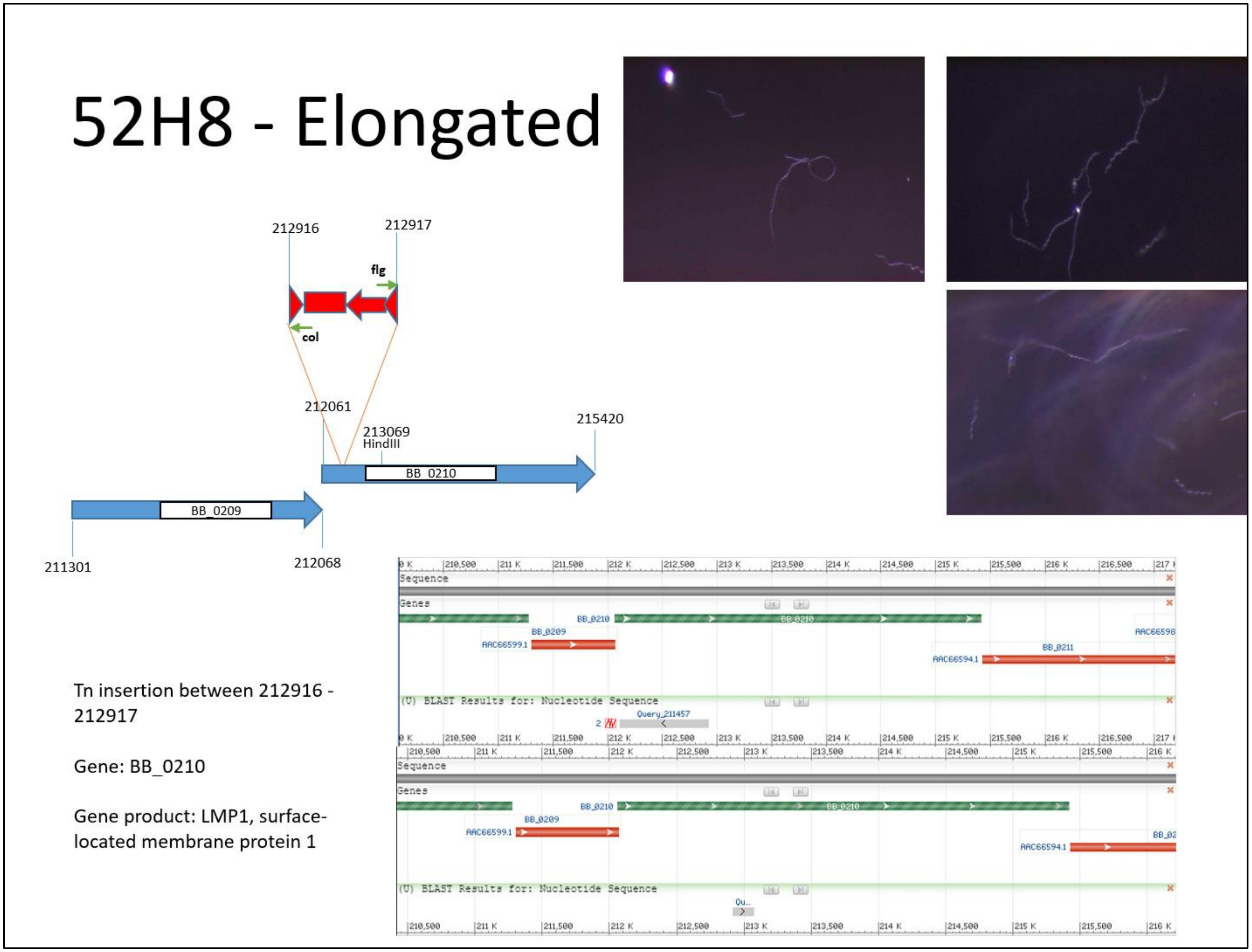
52H8 - Elongated
212916
212917
flg
col
212061
213069
HindIII
215420
BB_0210
BB_0209
211301
212068
Tn insertion between 212916 - 212917
Gene: BB_0210
Gene product: LMP1, surface-located membrane protein 1
Sequence
Genes
BB_0210
BB_0209
AAC66599.1
BB_0211
AAC66594.1
(U) BLAST Results for: Nucleotide Sequence
Query_211457

D

56H2 – Elongated, Defective spiral Aggregate

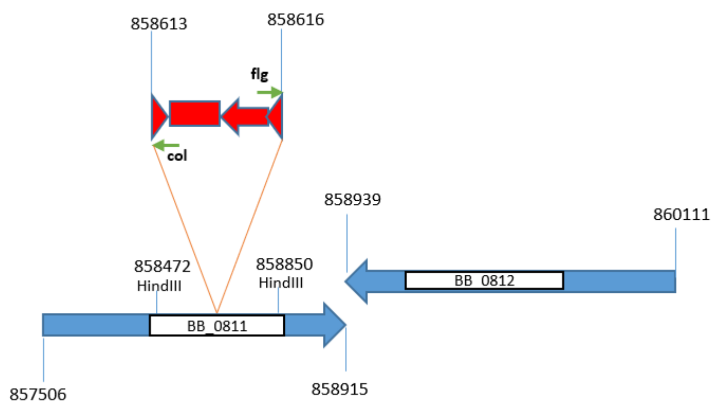

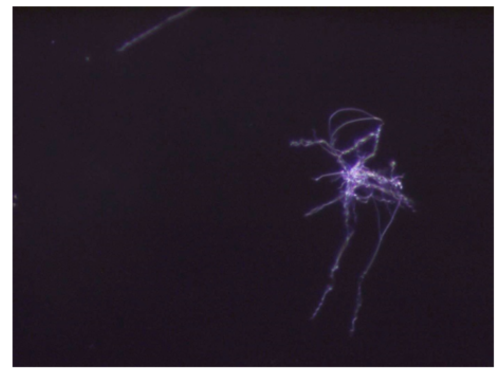

Tn insertion between 858613 and 858616

Gene: BB_0811

Gene product: Conserved hypothetical protein

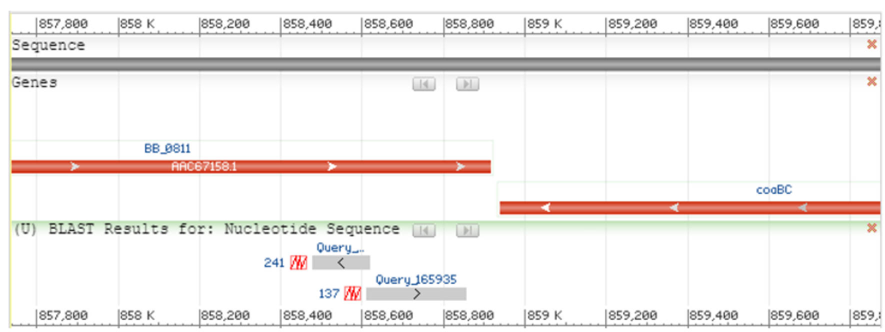

E

28F7 – Complete OspC deficiency

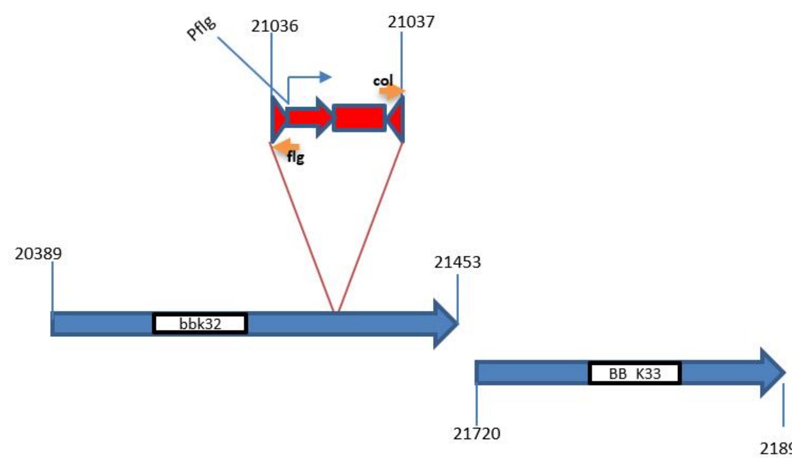

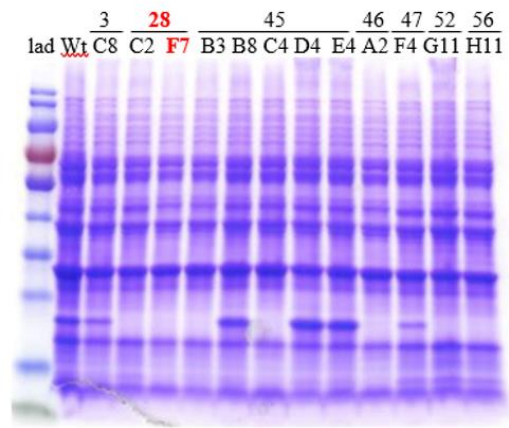

Insertion site: 21036-21037

Gene: bbk32

Gene product: fibronectin binding protein BBK32

F

45C4 – Complete OspC deficiency

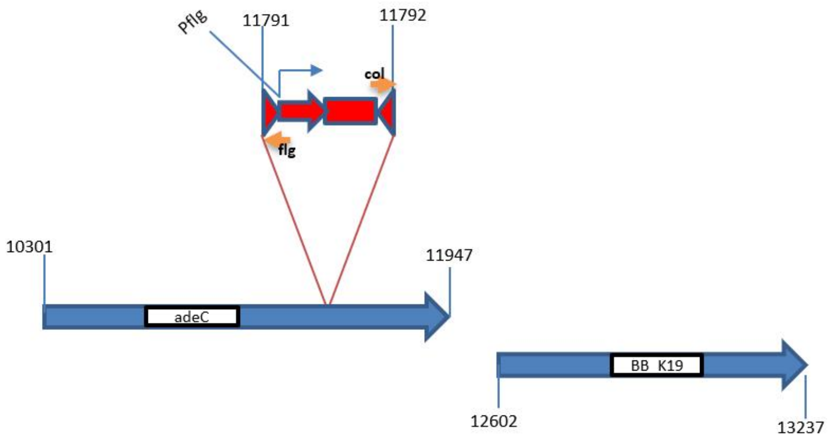

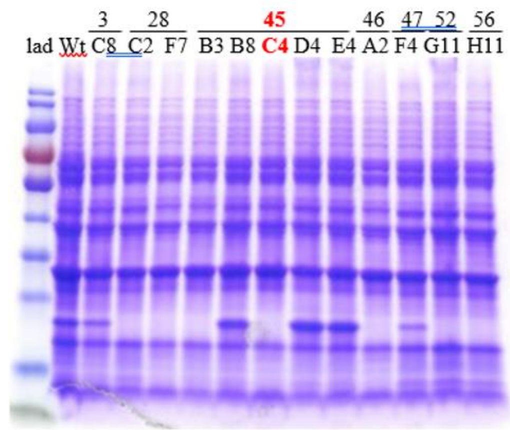

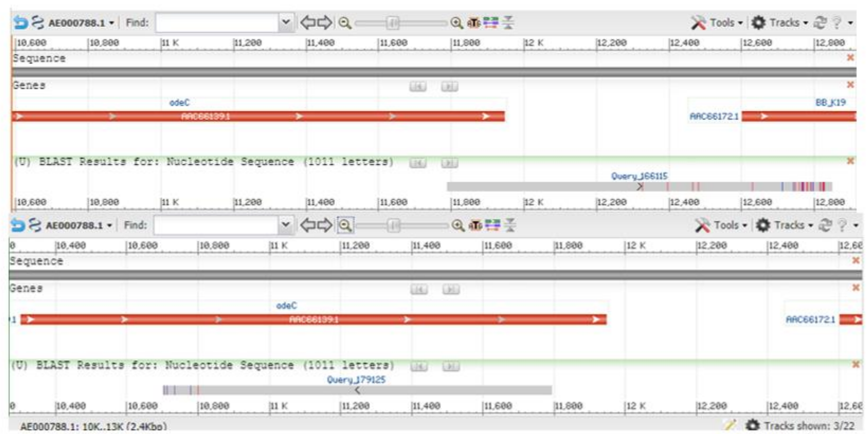

Insertion site: 11791-11792

Gene: adeC

Gene product: BBK17 Adenine deaminase

G

46A2 – Complete OspC deficiency

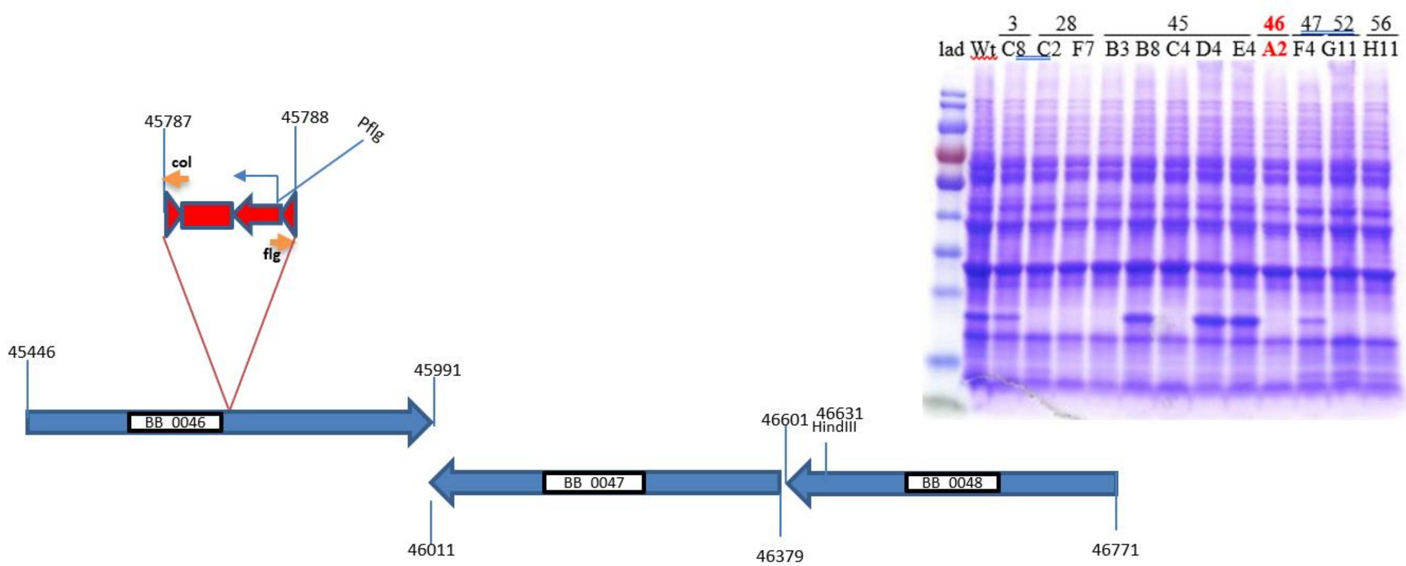

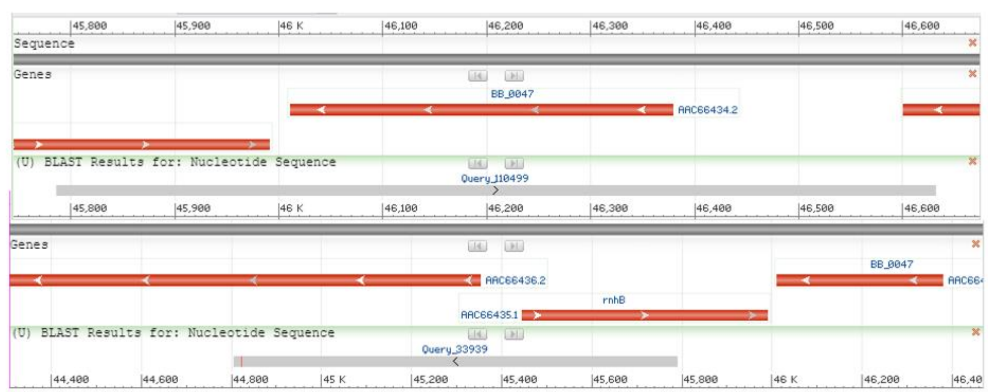

Insertion site: 45787 - 45788

Gene: BB_0046

Gene product: rnhB – ribonuclease HII

H

52G10 – Complete OspC deficiency

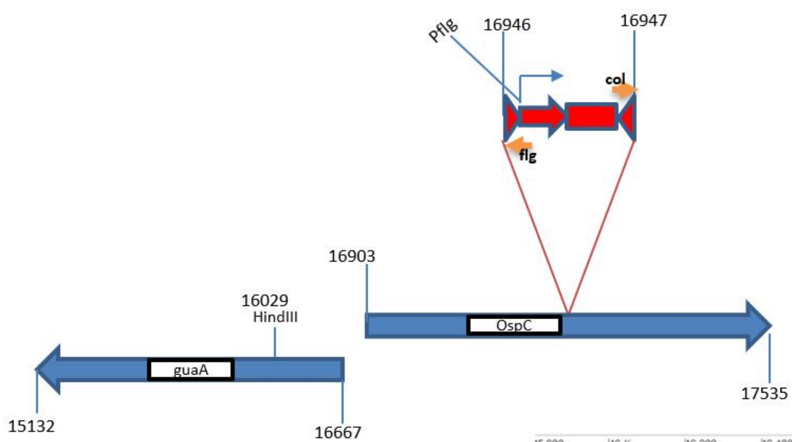

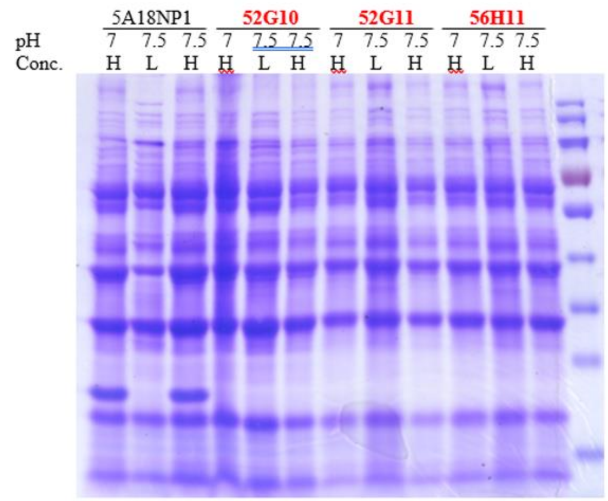

Insertion site: 16946-16947

Gene: OspC

Gene product: outer surface protein C

Figure 3.11: Transposon Insertion Sites of Sequenced Mutants

Col and flg reads were used with NCBI Blast to identify flanking regions of the transposon sequence. A-D, sequenced morphology mutants. E-H, sequenced OspC expression mutants. E-G: 28F7, 45C4, and 46A2 are indicated in red in the accompanying SDS-PAGE image. Multiple OspC expression mutants contained mutations in the *ospC* gene. 52G10 represents the sequencing results for these mutants. 52G11 and 56H11 had transposon insertion sites identical to 52G10.

DISCUSSION

From screening of approximately 1350 mutagenized samples, 85 potential morphology mutants and 66 potential OspC expression mutants have been found. While not all of these have a confirmed phenotype, they lay the groundwork for future investigations. The unconfirmed elongated, aggregate, and/or slow-growing mutants can undergo further microscopy analyses to provide visual and statistical evidence to their phenotypes. While only 40x magnification was used in this procedure, further endeavors can include higher magnification or enhanced microscopy procedures to characterize potential defective spiral mutants. Swarm agar assays in BSKII agar can be used to obtain quantifiable comparisons between Wt and potential motility mutants.

Of the OspC expression mutants, the main focus of the study was to identify mutants with complete OspC depletion. With over half of the OspC depleted mutants containing transposon insertions in the *ospC* gene itself (Table 3.5), the focus may shift to those with underexpressed or overexpressed OspC phenotypes. Further work will be conducted to verify the OspC expression phenotypes of the remaining OspC depleted mutants as well as the underexpressed and overexpressed phenotypes. This work includes repeated SDS-PAGEs and conditional SDS-PAGEs.

Of the 37 confirmed morphology mutants and the 8 confirmed OspC expression mutants, eleven samples have been successfully identified, cloned, and sequenced, resulting in the identification of both novel and previously discovered genes. As detailed earlier, three of the morphology mutants resulted in putative/hypothetical proteins (Table 3.5). These samples will undergo complementation to confirm the relationship between the gene and its observed phenotype. Plasmid profiling will be used to confirm the observed phenotypes are not due to loss of any plasmids. Upon confirmation of genotypic link to the phenotype, studies should be performed to characterize the structure of the protein and potential biochemical interactions. Information obtained from these studies may help determine how these proteins function and produce the observed phenotype within the organism.

LMP1, the mutated gene in 52H8 (Table 3.5, Figure 3.11D), has been identified in other studies as a membrane protein required to resist or evade the host-adaptive immune response (Kenedy *et al,* 2012; Koci *et al,* 2018; Yang *et al,* 2009; Yang *et al,* 2010). However, none of these studies compared morphologies or noted morphological mutants during their work. As morphologies of *B. burgdorferi* can be affected by various changes in environment, such as inadequate nutritional media (Barbour *et al,* 1986), careful analysis of morphology is suggested while continuing knock-out/complementation work on this gene.

The four identified genes from the OspC depleted mutants consist of *bbk32, bbk17* (also known as *adeC*), *rnhB,* and *ospC.* The BBK32 protein has already been extensively studied and identified as a surface protein of *B. burgdorferi* that plays an important role in the attachment of the spirochetes to the extracellular matrix and is required for optimal infectivity of the organism (Fischer *et al,* 2006; Hyde *et al,* 2011b; Probert and Johnson, 1998). It is more highly expressed during tick feeding and mammalian infection and has lower expression in flat, unfed ticks (Fikrig *et al,* 2000; Li *et al,* 2006). More importantly, it has been found to illicit protective host immune activity and its inactivation decreases the infectivity of *B. burgdorferi* (Fikrig *et al,* 1997; Seshu *et al,* 2006). The combination of all these factors led to the discovery that BBK32 is in fact controlled by the Rrp2-

RpoN-RpoS pathway alongside OspC (He *et al*, 2007). While the mechanisms controlling for BBK32 have been studied, no studies have been performed to identify if BBK32 controls expression of OspC. Experiments should be performed to distinguish if the loss of OspC is indeed controlled by loss of BBK32. If so, further experimentation should be done to determine the molecular processes behind this control.

BBK17 has also been previously studied, though not to the extent of BBK32. BBK17, or adeC, was identified as an important contributor to mammalian infectivity and its inactivation attenuates *B. burgdorferi* infection in mice (Jewett *et al*, 2007). Unlike BBK32, no connection has been made between adeC and the RpoN-RpoS pathway. It has so far only been characterized as an adenine deaminase required for the direct deamination of adenine to produce hypoxanthine, a purine derivative important for the salvage and metabolism of adenine in many prokaryotic species (Jewett *et al*, 2007; Nygaard *et al*, 1996). Hypoxanthine is the most abundant purine in mammalian blood and its transport may be critical during the initial stages of Borrelial infectivity (Hartwick *et al,* 1979; Jain *et al*, 2012). Further studies would need to be performed in order to establish a relationship between adeC and the OspC expression phenotype, to establish a relationship between adeC and the RpoN-RpoS pathway, and to identify any effects of adeC on infectivity and pathogenesis of the organism.

The third gene found associated with depleted OspC expression was *rnhB,* ribonuclease HII, that has been predicted to specifically degrade the RNA of RNA-DNA hybrids (Ohtani *et al,* 1999). The gene product and its function in *B. burgdorferi* has so far only been predicted from sequence homology (Fraser *et al*, 1997) and has not been studied further. Ribonucleases have a wide variety of potential functions involving bacterial RNA metabolism, such as switching pre-RNA to functional RNAs, mRNA regulation, mRNA degradation, or controlling regulatory RNAs (Deutscher, 2006; 2015; Esquerre *et al*, 2014). Ribonuclease HII, or RNase HII, is a temperature-sensitive enzyme whose activity is dependent on the presence of Mn^{2+} (Ohtani *et al*, 1999). This is particularly intriguing as Mn^{2+} plays a critical role in the regulation of the RpoS pathway controlling OspC expression (Troxell *et al*, 2013). However, it should be noted that activity of RNase HII is positively correlated with the presence of Mn^{2+} while the presence of Mn^{2+} is inversely correlated with the presence of OspC. This makes our findings particularly confusing as the loss of RNase HII results in depletion of OspC.

In terms of physiological roles, RNase H's have been widely studied in *E. coli* but with stronger focus on RNase HI as opposed to RNase HII. Thus far, researchers have hypothesized that RNase HII is responsible for excising misincorporated ribonucleotides in DNA as a type of DNA repair (Rydberg and Game, 2002). This role may hold true in some cases, but it does not adequately explain the link between the enzyme and OspC expression seen here. RNase HII is also believed to constitute a significant part of the RNA degradosome complex in *E. coli*. Its primary role appears to be the degradation of mRNA (Lu and Taghbalout, 2014). It is possible that RNase HII holds a similar role in *B. burgdorferi*, either on its own or in conjunction with a previously undiscovered degradosome complex, in order to aid in RNA processing and/or degradation.

As with the rest of the identified genes, complementation would be used to ensure a link between the observed phenotype and the *rnhB* gene. With the tendency for RNases to regulate gene expression, this gene will be particularly interesting to explore in relation to RpoN, RpoS, and OspC levels. Due its strong association with other degradosome proteins in *E. coli*, it may be a good idea to search for other degradosome proteins present in *B. burgdorferi*. Any that are found should be analyzed for associations with RNase HII and effects on OspC expression. Immunofluorescence experiments would be recommended regardless of the presence of other degradosome proteins in order to identify which factors in the RpoN-RpoS pathway may be affected by this enzyme. Studies should be performed to characterize biochemical and molecular interactions of this enzyme that effect this pathway.

For all identified mutants, procedures such as Western blots and plasmid profiling would be necessary to confirm the causal relationship of the genotype to the phenotype. Using complementation procedures with Western blotting would allow for evaluation of the role of the identified gene in relation to its protein expression. Plasmid profiling is an essential step in verifying a genotype-phenotype link due to *B. burgdorferi*'s spontaneous loss of plasmids when growing *in vitro*. This process allows us to visualize all the plasmids present within the sample compared to wildtype and allows us to verify that the observed phenotype is not due to a missing plasmid. The plasmid profiling process can also lead to novel discoveries involving plasmids, rather than genes, found responsible for certain phenotypes. For example, preliminary data from Dr. Raghunandanan in the Yang Lab has shown that at least three OspC deficient mutants are missing plasmid lp21. Additionally, the genes identified from sequencing did not return Wt phenotype after complementation. This discovery is intriguing as lp21 has previously been thought to be unnecessary.

APPENDIX A: List of All Potential Mutants by Plate Number

Sample	Phenotype	Confirmation	Insertion Site/Gene
Plate 1			
1A8	Elongated	Via imaging and stats analysis	n/a
1B5	Elongated and slow-growing	Via imaging, growth curves, and stats analysis	n/a
1D12	OspC Overexpression	Unconfirmed	n/a
1E10	Slow-growing	Via growth curves and stats analysis	n/a
1E12	Increased motility	Unconfirmed	n/a
1F5	OspC Underexpression	Unconfirmed	n/a
1G4	Aggregate	Via imaging and stats analysis	n/a
1H12	Elongated	Via imaging and stats analysis	n/a
Plate 2			
2A6	OspC Overexpression	Unconfirmed	n/a
2A9	OspC Overexpression	Unconfirmed	n/a
2A10	OspC Overexpression	Unconfirmed	n/a
2A12	OspC Overexpression	Unconfirmed	n/a
2B1	Increased motility	Unconfirmed	n/a

2B6	OspC Overexpression	Unconfirmed	n/a
2B11	OspC Overexpression	Unconfirmed	n/a
2B12	OspC Overexpression	Unconfirmed	n/a
2C1	Elongated and slow-growing	Unconfirmed	n/a
2D1	Elongated	Via imaging and stats analysis	n/a
2D12	OspC Overexpression	Unconfirmed	n/a
2E7	Elongated	Via imaging and stats analysis	n/a
2G11	OspC Overexpression	Unconfirmed	n/a
2H1	Elongated and defective spiral	Via imaging and stats analysis	n/a
2H7	OspC Overexpression	Unconfirmed	n/a
2H12	OspC Overexpression	Unconfirmed	n/a
Plate 3			
3B2	OspC Overexpression	Unconfirmed	n/a
3B4	Elongated and defective spiral	Unconfirmed	n/a
3B5	Elongated	Unconfirmed	n/a
3C6	Decreased motility	Unconfirmed	n/a
3D2	OspC Overexpression	Unconfirmed	n/a

3D3	OspC Overexpression	Unconfirmed	n/a
3D10	Elongated	Unconfirmed	n/a
3E5	Elongated and defective spiral	Unconfirmed	n/a
3E8	Elongated	Via imaging and stats analysis	n/a
3E9	Increased motility	Unconfirmed	n/a
3E12	Defective spiral	Unconfirmed	n/a
3F3	Elongated and defective spiral	Unconfirmed	n/a
3F10	Elongated and defective spiral OspC Underexpression	Via imaging and stats analysis Unconfirmed	n/a
3F12	OspC Overexpression	Unconfirmed	n/a
3H2	Elongated	Via imaging and stats analysis	n/a
3H3	OspC Overexpression	Unconfirmed	n/a
Plate 5			
5A7	Elongated, defective spiral, slow-growing	Via imaging and stats analysis; Slow-growth phenotype unconfirmed	n/a
5C2	Slow-growing	Via growth curve and stats analysis	n/a
5D2	Elongated	Via imaging and stats analysis	n/a
5D4	Elongated	Via imaging and stats analysis	n/a

5F11	Elongated	Via imaging and stats analysis	n/a
5G11	Elongated, defective spiral, and decreases motility	Via imaging and stats analysis; Motility phenotype unconfirmed	n/a
Plate 7			
7A10	Elongated and aggregate	Via imaging and stats analysis	BB_0043: unknown predicted protein coding gene
7B12	Slow-growing	Unconfirmed	n/a
7D8	Elongated	Via imaging and stats analysis	n/a
7D11	Elongated	Via imaging and stats analysis	n/a
7F7	Elongated and defective spiral	Unconfirmed	n/a
7F10	Elongated and defective spiral	Unconfirmed	n/a
7H11	Elongated	Via imaging and stats analysis	n/a
Plate 28			
28A8	OspC Overexpression	Unconfirmed	n/a
28B8	Defective spiral	Unconfirmed	n/a
28C2	Complete OspC deficiency	Via repeated SDS-PAGE	n/a
28C4	Increased motility OspC Overexpression	Unconfirmed Unconfirmed	n/a

28C11	Defective spiral	Unconfirmed	n/a
28E12	Defective spiral	Unconfirmed	n/a
28F7	Complete OspC deficiency	Via repeated SDS-PAGE	Bbk32: Fibronectin-binding protein
28G9	OspC Overexpression	Unconfirmed	n/a
Plate 45			
45A5	OspC Underexpression	Unconfirmed	n/a
45B2	OspC Overexpression	Unconfirmed	n/a
45B3	Aggregate Complete OspC deficiency	Via imaging and stats analysis Via repeated SDS-PAGE	BB_B19: Outer surface protein C
45B11	OspC Underexpression	Unconfirmed	n/a
45B12	OspC Underexpression	Unconfirmed	n/a
45C2	OspC Underexpression	Unconfirmed	n/a
45C4	Complete OspC deficiency	Via repeated SDS-PAGE	BB_K17: Adenine deaminase C
45C7	Increased motility OspC Overexpression	Unconfirmed Unconfirmed	n/a
45C8	OspC Underexpression	Unconfirmed	n/a
45C9	OspC Underexpression	Unconfirmed	n/a

45C10	OspC Overexpression	Unconfirmed	n/a
45D1	OspC Underexpression	Unconfirmed	n/a
45D5	Elongated and defective spiral	Via imaging and stats analysis	n/a
45D7	Elongated and defective spiral	Via imaging and stats analysis	n/a
45E7	OspC Underexpression	Unconfirmed	n/a
45E9	OspC Underexpression	Unconfirmed	n/a
45E11	OspC Underexpression	Unconfirmed	n/a
45F5	Complete OspC deficiency	Unconfirmed	n/a
45F12	Elongated	Unconfirmed	n/a
45H4	OspC Underexpression	Unconfirmed	n/a
45H9	Increased motility	Unconfirmed	n/a
45H11	Elongated	Unconfirmed	n/a
Plate 46			
46A2	Complete OspC deficiency	Via repeated SDS-PAGE	BB_0046: Ribonuclease HII
46F5	Elongated	Via imaging and stats analysis	n/a
46F10	Elongated	Via imaging and stats analysis	n/a

Plate 47			
47A6	OspC Underexpression	Unconfirmed	n/a
47A9	Slow-growing	Unconfirmed	n/a
47B3	Elongated	Via imaging and stats analysis	n/a
47B5	OspC Underexpression	Unconfirmed	n/a
47D11	OspC Underexpression	Unconfirmed	n/a
47E5	OspC Underexpression	Unconfirmed	n/a
47E11	Aggregate	Via imaging and stats analysis	n/a
47F1	OspC Underexpression	Unconfirmed	n/a
47F6	OspC Underexpression	Unconfirmed	n/a
47G11	Increased motility	Unconfirmed	n/a
Plate 48			
48C1	Elongated	Via imaging and stats analysis	BB_0420: Sensory transduction histidine kinase, putative
48D4	Defective spiral and decreased motility	Unconfirmed	n/a
48G9	Elongated, defective spiral, and slow-growing	Via imaging, growth curves, and stats analysis	n/a

48H5	Slow-growing	Via growth curves and stats analysis	n/a
48H12	OspC Overexpression	Unconfirmed	n/a
Plate 52			
52A11	Decreased motility	Unconfirmed	n/a
52D1	OspC Overexpression	Unconfirmed	n/a
52D9	Elongated	Unconfirmed	n/a
52D12	OspC Overexpression	Unconfirmed	n/a
52E10	Elongated, defective spiral, and slow-growing	Via imaging, growth curve, and stats analysis	n/a
52E12	OspC Overexpression	Unconfirmed	n/a
52G10	Complete OspC deficiency	Via repeated SDS-PAGE	BB_B19: Outer surface protein C
52G11	Complete OspC deficiency	Via repeated SDS-PAGE	BB_B19: Outer surface protein C
52H8	Elongated	Via imaging and stats analysis	BB_0210: LMP1, surface-located membrane protein 1
Plate 54			
54A1	Slow-growing	Unconfirmed	n/a
54A2	Slow-growing	Unconfirmed	n/a

54E3	Elongated	Unconfirmed	n/a
54G1	Elongated	Unconfirmed	n/a
54G6	Elongated and aggregate	Unconfirmed	n/a
54H10	Elongated and aggregate	Unconfirmed	n/a
Plate 56			
56A12	Elongated and aggregate	Unconfirmed	n/a
56D12	Elongated and aggregate	Unconfirmed	n/a
56E9	Elongated	Via imaging and stats analysis	n/a
56F5	Elongated, defective spiral, and aggregate	Via imaging and stats analysis	n/a
56F9	Increased motility	Unconfirmed	n/a
56H2	Elongated, defective spiral, aggregate	Via imaging and statistical analysis	BB_0811: Conserved hypothetical protein
56H11	Complete OspC deficiency	Via repeated SDS-PAGE	BB_B19: Outer surface protein C
Plate 62			
62A2	Complete OspC deficiency	Unconfirmed	n/a
62A5	Elongated and aggregate	Via imaging and stat analysis	n/a

62A6	Elongated	Unconfirmed	n/a
62B2	Elongated	Unconfirmed	n/a
62B3	Complete OspC deficiency	Unconfirmed	n/a
62B4	OspC Overexpression	Unconfirmed	n/a
62B6	Elongated and aggregate	Unconfirmed	n/a
62C4	Elongated	Unconfirmed	n/a
62C5	Increased motility	Unconfirmed	n/a
62C6	Elongated and aggregate	Via imaging and stats analysis	n/a
62C7	Defective spiral	Unconfirmed	n/a
62C8	Defective spiral	Unconfirmed	n/a
62D5	Defective spiral and increased motility	Unconfirmed	n/a
62E3	Complete OspC deficiency	Unconfirmed	n/a
62F3	OspC Overexpression	Unconfirmed	n/a
62F4	OspC Overexpression	Unconfirmed	n/a
62F6	Increased motility	Unconfirmed	n/a
62G5	Elongated	Unconfirmed	n/a

62H1	OspC Overexpression	Unconfirmed	n/a
62H4	Elongated	Unconfirmed	n/a
62H5	Complete OspC deficiency	Unconfirmed	n/a

REFERENCES

1. Barbour AG. 1984. Isolation and cultivation of Lyme disease spirochetes. Yale J Biol Med 57: 521-525.

2. Barbour AG, Hayes SF. 1986. Biology of *Borrelia* Species. Microbiol Rev 50: 381-400.

3. Blevins JS, Xu H, He M, Norgard MV, Reitzer L, Yang XF. 2009. Rrp2, a σ^{54}-Dependent Transcriptional Activator of *Borrelia burgdorferi,* Activates *rpoS* in an Enhancer-Independent Manner. J Bacteriol 191: 2902-2905.

4. Boardman BK, He M, Ouyang Z, Xu H, Pang X, Yang XF. 2008. Essential Role of the Response Regulator Rrp2 in the Infectious Cycle of *Borrelia burgdorferi*. Infect Immun 76: 3844-3853.

5. Boylan JA, Posey JE, Gherardini FC. 2003. *Borrelia* oxidative stress response regulator, BosR: A distinctive Zn-dependent transcriptional activator. Proc Natl Acad Sci USA 100: 11684-11689.

6. Brisson D, Drecktrah D, Eggers CH, Samuels DS. 2012. Genetics of *Borrelia burgdorferi*. Annu Rev Genet 46: 515-536.

7. Burgdorfer W, Barbour AG, Hayes SF, Benach JL, Gurnwaldt E, David JP. 1982. Lyme disease—a tick-borne spirochetosis? Science 216: 1317-1319.

8. Burgdorfer W. 1991. Lyme borreliosis: ten years after discovery of the etiologic agent, Borrelia burgdorferi. Infection 19: 257-62.

9. Burtnick MN, Downey JS, Brett PJ, Boylan JA, Frye JG, Hoover TR, Gherardini FC. 2007. Insights into the complex regulation of *rpoS* in *Borrelia burgdorferi.* Mol Microbiol 65: 277-293.

10. Caimano MJ, Eggers CH, Hazlett KRO, Radolf JD. 2004. RpoS Is Not Central to the General Stress Response in *Borrelia burgdorferi* but Does Control Expression of One or More Essential Virulence Determinants. Infect Immun 72: 6433-6445.

11. Carrasco SE, Troxell B, Yang Y, Brandt SL, Li H, Sandusky GE, Condon KW, Serezani CH, Yang XF. 2015. Outer surface protein OspC is an antiphagocytic factor that protects Borrelia burgdorferi from phagocytosis by macrophages. Infect Immun 83: 4848-4860.

12. Casjens S, Palmer N, Van Vugt R, Huang WM, Stevenson B, Rosa P, Lathigra R, Sutton G, Peterson J, Dodson RJ, Haft D, Hickey E, Gwinn M, White O, Fraser CM.

2002. A bacterial genome in flux: the twelve linear and nine circular extrachromosomal DNAs in an infectious isolate of the Lyme disease spirochete *Borrelia burgdorferi.* Mol Microbiol 35: 490-516.

13. CDC. 2018a. How many people get Lyme disease? Accessed: Jan 21, 2019. https://www.cdc.gov/lyme/stats/humancases.html

14. CDC. 2018b. Lyme Disease Chart and Figures: Historical Data. Accessed: Jan 21, 2019. https://www.cdc.gov/lyme/stats/graphs.html

15. CDC. 2018c. Lyme Disease: Signs and symptoms. Accessed: Jan 19, 2019. https://www.cdc.gov/lyme/signs_symptoms/index.html

16. CDC. 2018d. Lyme Disease Treatment. Accessed: April 3, 2019. https://www.cdc.gov/lyme/treatment/index.html

17. CDC. 2019. Lyme Disease: Data and Surveillance. Accessed: January 21, 2019. https://www.cdc.gov/lyme/datasurveillane/index.html

18. Chaconas G, Kobryn K. 2010. Structure, function, and evolution of linear replicons in Borrelia. Annu Rev Microbiol 64: 185-202.

19. Charon NW, Goldstein SF. 2002. Genetics of Motility and Chemotaxis of a Fascinating Group of Bacteria: The Spirochetes. Annu Rev Genet 36: 47-73.

20. Charon NW, Cockburn A, Li C, Liu J, Miller KA, Miller MR, Motaleb MD, Wolgemuth CW. 2012. The unique paradigm of spirochete motility and chemotaxis. Annu Rev Microbio 66: 349-370.

21. Cooke WD, Dattwyler RJ. 1992. Complications of Lyme Borreliosis. Ann Rev Med 43: 93-103.

22. Deutscher MP. 2006. Degradation of RNA in bacteria: comparison of mRNA and stable RNA. Nucleic Acids Res 34: 659-666.

23. Deutscher MP. 2015. How bacterial cells keep ribonucleases under control. FEMS Microbiol Rev 39: 350-361.

24. Di Domenico EG, Cavallo I, Bordignon V, D'Agosto, Pontone M, Trento E, Gallo MT, Prignano G, Pimpinelli F, Toma L, Ensoli F. 2018. The Emerging Role of Microbial Biofilm in Lyme Neuroborreliosis. Front Neurol 9: 1048.

25. Dunham-Ems SM, Caimano MJ, Pal U, Wolgemuth CW, Eggers CH, Balic A, Radolf JD. 2009. Live imaging reveals a biphasic mode of dissemination of *Borrelia burgdorferi* within ticks. J Clin Invest 119: 3652-3665.

26. Esquerre T, Laguerre S, Turlan C, Carpousis AJ, Girbal L, Cocaign-Bousquet M. 2014. Dual role of transcription and transcript stability in the regulation of gene expression in Escherichia coli cells cultured on glucose at different growth rates. Nucleic Acids Res 42: 2460-2472.

27. Fikrig E, Barthold SW, Sun W, Feng W, Telford III SR, Flavell RA. 1997. Borrelia burgdorferi P35 and P37 proteins, expressed in vivo, elicit protective immunity. Immunity 6: 531-539.

28. Fikrig E, Feng W, Barthold SW, Telford III SR, Flavell RA. 2000. Arthropod- and Host-Specific *Borrelia burgdorferi bbk32* Expression and the Inhibition of Spirochete Transmission. J Immunol 164: 5344-5351.

29. Fischer JR, LeBlanc KT, Leong JM. 2006. Fibronectin Binding Protein BBK32 of the Lyme Disease Spirochete Promotes Bacterial Attachment to Glycosaminoglycans. Infect Immun 74: 435-441.

30. Fisher MA, Grimm D, Henion AK, Stewart PE, Rosa PA, Gherardini FC. 2005. Borrelia burgdorferi σ^{54} is required for mammalian infection and vector transmission but not for tick colonization. Proc Natl Acad Sci USA 102: 5162-5167.

31. Fraser CM, Casjens S, Huang WM, Sutton GG, Clayton R, Lathigra R, White O, Ketchum KA, Dodson R, Hickey EK, Gwinn M, Dougherty B, Tomb JF, Fleischmann RD, Richardson D, Peterson J, Kerlavage AR, Quackenbush J, Salzberg S, Hanson M, van Vugt R, Palmer N, Adams MD, Gocayne J, Weidman J, Utterback T, Watthey L, McDonald L, Artiach P, Bowman C, Garland S, Fujii C, Cotton MD, Horst K, Roberts K, Hatch B, Smith HO, Venter JC. 1997. Genomic sequence of a Lyme disease spirochaete, *Borrelia burgdorferi*. Nature 390: 580-586.

32. Ge Y, Li C, Corum L, Slaughter CA, Charon NW. 1998. Structure and Expression of the FlaA Periplasmic Flagellar Protein of *Borrelia burgdorferi.* J Bacteriol 180: 2418-2425.

33. Gray, JS. 1998. Review: The ecology of ticks transmitting Lyme borreliosis. Experimental & Applied Acarology 22: 249-258.

34. Grimm D, Tilly K, Byram R, Stewart PE, Krum JG, Bueschel DM, Schwan TG, Policastro PF, Elias AF, Rosa PA. 2004. Outer-surface protein C of the Lyme disease spirochete: A protein induced in ticks for infection of mammals. PNAS 101: 3142-3147.

35. Haake DA. 2000. Spirochaetal lipoproteins and pathogenesis. Microbiology 146: 1491-1504.

36. Hartwick RA, Assenza SP, Brown PR. 1979. Identification and quantitation of nucleosides, bases, and other UV-absorbing compounds in serum, using reversed-

phase high-performance liquid chromatography. I. Chromatographic methodology. J Chromatogr 186: 647-658.

37. He M, Boardman BK, Yan D, Yang XF. 2007. Regulation of Expression of the Fibronectin-Binding Protein BBK32 in *Borrelia burgdorferi*. J Bacteriol 189: 8377-8380.

38. Hubner A, Yang XF, Nolen DM, Popova TG, Cabello FC, Norgard MV. 2001. Expression of *Borrelia burgdorferi* OspC and DbpA is controlled by a RpoN-RpoS regulatory pathway. PNAS 22: 12724-12729.

39. Hyde JA, Shaw DK, Smith III R, Trzeciakowski JP, Skare JT. 2009. The BosR regulatory protein of *Borrelia burgdorferi* interfaces with the RpoS regulatory pathway and modulates both the oxidative stress response and pathogenic properties of the Lyme disease spirochete. Mol Microbiol 74: 1344-1355.

40. Hyde JA, Weening EH, Skare JT. 2011a. Genetic Manipulation of *Borrelia burgdorferi*. Curr Protocol Microbiol 20: 12C.4.1-12C.4.17.

41. Hyde JA, Weening EH, Chang M, Trzeciakowski JP, Hook M, Cirillo JD, Skare JT. 2011b. Bioluminescent imaging of Borrelia burgdorferi in vivo demonstrates that the fibronectin-binding protein BBK32 is required for optimal infectivity. Mol Microbiol 82: 99-113.

42. Jain S, Sutchu, S, Rosa PA, Byram R, Jewett MW. 2012. *Borrelia burgdorferi* Harbors a Transport System Essential for Purine Salvage and Mammalian Infection. Infect Immun 80: 3086-3093.

43. Jewett MW, Lawrence K, Bestor AC, Tilly K, Grimm D, Shaw P, VanRaden M, Gherardini F, Rosa PA. 2007. The critical role of the linear plasmid lp36 in the infectious cycle of *Borrelia burgdorferi*. Mol Microbiol 64: 1358-1374.

44. Johnson RC. 1977. The Spirochetes. Ann Rev Microbiol 31: 89-106.

45. Johnson RC, Schmid GP, Hyde FW, Steigerwalt AG, Brenner DJ. 1984. *Borrelia burgdorferi* sp. nov.: Etiologic Agent of Lyme Disease. Int J Syst Bacteriol 34: 496-497.

46. Kenedy MR, Lenhart TR, Akins DR. 2012. The Role of *Borrelia burgdorferi* Outer Surface Proteins. FEMS Immunol Med Microbiol 66: 1-19.

47. Kobryn K, Chaconas G. 2002. ResT, a telomere resolvase encoded by the Lyme disease spirochete. Mol Cell 9: 195-201.

48. Koci J, Bernard Q, Yang X, Pal U. 2018. *Borrelia burgdorferi* surface protein Lmp1 facilitates pathogen dissemination through ticks as studies by an artificial membrane feeding system. Sci Rep 8: 1910.

49. Labandeira-Ray M, Skare JT. 2001. Decreased infectivity in Borrelia burgdorferi strain B31 is associated with loss of linear plasmid 25 or 28-1. Infect Immun 69: 446-455.

50. Li X, Liu X, Beck DS, Kantor FS, Fikrig E. 2006. *Borrelia burgdorferi* Lacking BBK32, a Fibronectin-Binding Protein, Retains Full Pathogenicity. Infect Immun 74: 3305-3313.

51. Li C, Xu H, Zhang K, Liang FT. 2010. Inactivation of a putative flagellar motor switch protein FliG1 prevent *Borrelia burgdorferi* from swimming in highly viscous media and blocks its infectivity. Mol Microbiol 75: 1563-1576.

52. Lu F, Taghbalout A. The *Escherichia coli* major exoribonclease RNase II is a component of the RNA degradosome. Biosci Rep 34: e00166.

53. Lybecker MC, Abel CA, Feig AL, Samuels DS. 2010. Identification and function of the RNA chaperone Hfq in the Lyme disease spirochete *Borrelia burgdorferi*. Mol Microbiol 78: 622-635.

54. Marques A. 2008. Chronic Lyme Disease: An appraisal. Infect Dis Clin North Am 22: 341-360.

55. McBride A, Athanazio D, Reis M, Ko A. 2005. Leptospirosis. Current Opinion in Infectious Diseases. 18: 376-386.

56. Merilainen L, Herranen A, Schwarzbach A, Gilbert L. 2015. Morphological and biochemical features of *Borrelia burgdorferi* pleomorphic forms. Microbiology 161: 516-527.

57. Miller CL, Rajasekhar Karna SL, Seshu J. 2013. *Borrelia* host adaptation Regulator (BadR) regulates *rpoS* to modulate host adaptation and virulence factors in *Borrelia burgdorferi*. Mol Microbiol 88: 105-124.

58. Motaleb MA, Corum L, Bono JL, Elias AF, Rosa P, Samuels DS, Charon NW. 2000. *Borrelia burgdorferi* periplasmic flagella have both skeletal and motility functions. Proc Natl Acad Sci U S A 97: 10899-10904.

59. Motaleb MA, Miller MR, Li C, Bakker RG, Goldstein SF, Silversmith RE, Bourret RB, Charon NW. 2005. CheX is a phosphorylated CheY phosphatase essential for Borrelia burgdorferi chemotaxis. J Bacteriol 187: 7963-7969.

60. Motaleb MA, Sultan SZ, Miller MR, Li C, Charon NW. 2011. CheY3 of *Borrelia burgdorferi* Is the Key Response Regulator Essential for Chemotaxis and Forms a Long-Lived Phosphorylated Intermediate. J Bacteriol 193: 3332-3341.

61. Motaleb MA, Liu J, Wooten RM. 2015. Spirochetal motility and chemotaxis in the natural enzootic cycle and development of Lyme disease. Current Opinion in Microbiology 28: 106-13.

62. Nygaard P, Duckert P, Saxild HH. 1996. Role of adenine deaminase in purine salvage and nitrogen metabolism and characterization of the ade gene in Bacillus subtilis. J Bacteriol 178: 846-853.

63. Ohtani N, Haruki M, Morikawa M, Crouch RJ, Itaya M, Kanaya S. 1999. Identification of the Genes Encoding Mn^{2+}-Dependent RNase HIII from *Bacillus subtilis*: Classification of RNases H into Three Families. Biochemistry 38: 605-618.

64. Ouyang Z, Kumar M, Kariu T, Hag S, Goldberg M, Pal U, Norgard MV. 2009. BosR (BB0647) governs virulence expression in Borrelia burgdorferi. Mol Microbiol 74: 1331-1343.

65. Ouyang Z, Deka RK, Norgard MV. 2011. BosR (BB0647) Controls the RpoN-RpoS Regulatory Pathway and Virulence Expression in *Borrelia burgdorferi* by a Novel DNA-Binding Mechanism. PLoS Pathog 7: e1001272.

66. Persat A, Stone HA, Gitai Z. 2014. The curved shape of Caulobacter crescentus enhances surface colonization in flow. Nat Commun 5: 3824.

67. Probert WS, Johnson BJ. 1998. Identification of a 47 kDa fibronectin-binding protein expressed by Borrelia burgdorferi isolate B31. Mol Microbiol 30: 1003-1015.

68. Purser JE, Lawrenz MB, Caimano MJ, Howell JK, Radolf JD, Norris SJ. 2003. A plasmid-encoded nicotinamidase (PncA) is essential for infectivity of Borrelia burgdorferi in a mammalian host. Mol Microbiol 48: 753-64.

69. Radolf JD. Treponema. In: Baron S, editor. Medical Microbiology. 4th edition. Galveston (TX): University of Texas Medical Branch at Galveston; 1996. Chapter 36. Available from: https://www.ncbi.nlm.nih.gov/books/NBK7716/

70. Radolf JD, Caimano MJ, Stevenson B, Hu LT. 2012.Of ticks, mice, and men: understanding the dual-host lifestyle of Lyme disease spirochaetes. Nat Rev Microbiol 10: 87-99.

71. Rosa PA, Tilly K, Stewart PE. 2005. The burgeoning molecular genetics of the Lyme disease spirochete. Nature Review Microbiology 3: 129-143.

72. Rydberg B, Game J. Excision of misincorporated ribonucleotides in DNA by RNase H (type 2) and FEN-1 in cell-free extracts. Proc Natl Acad Sci USA 99: 16654-16659.

73. Sal MS, Li C, Motalab MA, Shibata S, Aizawa SI, Charon NW. 2008. *Borrelia burgdorferi* Uniquely Regulates Its Motility Genes and Has an Intricate Flagellar Hook-Basal Body Structure. J Bacteriol 190: 1912-1921.

74. Sapi E, Theophilus PA, Pham TV, Burugu D, Luecke DF. 2016. Effect of RpoN, RpoS, and LuxS Pathways on the Biofilm formation and Antibiotic Sensitivity of *Borrelia burgdorferi*. Eur J Microbiol Immunol 6: 272-286.

75. Schmid GP. 1985. The global distribution of Lyme disease. Reviews of Infectious Diseases 7: 41-50.

76. Schwan TG, Piesman J, Golde WT, Dolan MC, Rosa PA. 1995. Induction of an outer surface protein on Borrelia burgdorferi during tick feeding. Proc Natl Acad Sci USA 92: 2909-2913.

77. Schwan TG, Piesman J. 2000. Temporal changes in outer surface proteins A and C of the Lyme disease-associated spirochete, Borrelia burgdorferi, during the chain of infection in ticks and mice. J Clin Microbiol 38: 382-388.

78. Seshu J, Esteve-Gessent MD, Labandeira-Rey M, Kim JH, Trzeciakowski JP, Hook M, Skare JT. 2006. Inactivation of the fibronectin-binding adhesin gene *bbk32* significantly attenuates the infectivity potential of *Borrelia burgdorferi.* Mol Microbiol 59: 1591-1601.

79. Setubal JC, Reis M, Matsunaga J, Haake DA. 2006. Lipoprotein computational prediction in spirochetal genomes. Microbiology 152: 113-121.

80. Smith AH, Blevins JS, Bachlani GN, Yang XF, Norgard MV. 2007. Evidence that RpoS (σ^S) in *Borrelia burgdorferi* is Controlled Directly by RpoN (σ^{54}/σ^N). J Bacteriol 189: 2139-2144.

81. Steere AC, Malawista SE, Snydman DR, Shope RE, Andiman WA, Ross MR, Steele FM. 1977. An epidemic of oligoarticular arthritis in children and adults in three Connecticut communities. Arthritis & Rheumatism 20: 7-17.

82. Steere AC, Broderick TF, Malawista SE. 1978. Erythema chronicum migrans and Lyme arthritis: epidemiologic evidence for a tick vector. American Journal of Epidemiology 108: 312-321.

83. Steere AC. 2001. Lyme Disease. N Engl J Med 345: 115-125.

84. Steere AC, Coburn J, Glickstein L. 2004. The emergence of Lyme disease. J Clin Invest 113: 1093-1101.

85. Stewart PE, Byram R, Grimm D, Tilly K, Rosa PA. 2004a. The plasmids of *Borrelia burgdorferi*: essential genetic elements of a pathogen. J Bacteriol 186: 3561-3569.

86. Stewart PE, Hoff J, Fischer E, Krum JG, Rosa PA. 2004b. Genome-Wide Transposon Mutagenesis of *Borrelia burgdorferi* for Identification of Phenotypic Mutants. Appl Environ Microbiol 70: 5973-5979.

87. Stewart PE, Rosa PA. 2008. Transposon mutagenesis of the Lyme disease agent *Borrelia burgdorferi.* Methods Mol Biol 431: 85-95.

88. Sultan SZ, Manne A, Stewart PE, Bestor A, Rosa PA, Charon NW, Motaleb MA. 2013. Motility is Crucial for the Infectious Life Cycle of *Borrelia burgdorferi*. Infect Immun 81: 2012-2021.

89. Sultan SZ, Sekar P, Zhao X, Manne A, Liu J, Wooten RM, Motaleb MA. 2015. Motor Rotation Is Essential for the Formation of the Periplasmic Flagellar Ribbon, Cellular Morphology, and *Borrelia burgdorferi* Persistence within *Ixodes scapularis* Tick and Murine Hosts. Infect Immun 83: 1765-1777.

90. Sze CW, Morado DR, Jun L, Charon NW, Hongbin X, Chunhao L. 2011. Carbon storage regulator A ($CsrA_{Bb}$) is a repressor of *Borrelia burgdorferi* flagellin protein FlaB. Mol Microbiol 82: 851-864.

91. Takayama K, Rothenburg RJ, Barbour AG. 1987. Absence of Lipopolysacchairde in the Lyme disease Spirochete, *Borrelia burgdorferi*. Infect Immun 55: 2311-2313.

92. Tilly K, Rosa PA, Stewart PE. 2008. Biology of Infection with *Borrelia burgdorferi*. Infect Dis Clin North Am 22: 217-234.

93. Troxell B, Ye M, Yang Y, Carrasco SE, Lou Y, Yang XF. 2013. Manganese and Zinc Regulate Virulence Determinants in *Borrelia burgdorferi*. Infect Immun 81: 2743-2752.

94. Wright WF, Riedel DJ, Talwani R, Gilliam BL. 2012. Diagnosis and Management of Lyme Disease. American Family Physician 85: 1086-1093.

95. Yang DC, Blair KM, Salama NR. 2016. Staying in Shape: the Impact of Cell Shape on Bacterial Survival in Diverse Environments. Microbiol Mol boil Rev 80: 187-203.

96. Yang XF, Goldberg MS, Popova TG, Schoeler GB, Wikel SK, Hagman KE, Norgard MV. 2002. Interdependence of environmental factors influencing reciprocal patterns of gene expression in virulent *Borrelia burgdorferi*. Mol Microbiol 37: 1470-1479.

97. Yang XF, Alani SM, Norgard MV. 2003. The response regulator Rrp2 is essential for the expression of major membrane lipoproteins in *Borrelia burgdorferi.* Proc Natl Acad Sci USA 100: 11001-11006.

98. Yang X, Coleman AS, Anguita J, Pal U. 2009. A Chromosomally Encoded Virulence Factor Protects the Lyme Disease pathogen against Host-Adaptive Immunity. PLoS Pathog 5: e1000326.

99. Yang X, Lenhart TR, Kariu T, Anguita J, Akins DR, Pal U. 2010. Characterization of Unique Regions of *Borrelia burgdorferi* Surface-Located Membrane Protein 1. Infect Immun 78: 4477-4487.

100. Ye M, Zhang JJ, Fang Z, Lawlis GB, Troxell B, Zhou Y, Gomelsky M, Lou Y, Yang XF. 2014. Dhhp, a cyclic di-AMP phosphodiesterase of Borellia burgdorferi, is essential for cell growth and virulence. Infect Immun 82: 1840-1849.

CURRICULUM VITAE

Amberly Nicole Grothe

Education

M.S. Microbiology & Immunology
IUPUI, Indianapolis, IN
August 2019

B.S. Biology
Abilene Christian University, Abilene, TX
May 2017

Honors and Awards

Phi Eta Sigma Honor Society
Abilene Christian University
2014

Research

IUSM Dept. of Microbiology & Immunology
Graduate Researcher in Dr. Frank Yang lab, 2017-2019
Project: "Identifying factors controlling cell shape and virulence gene expression in *Borrelia burgdorferi"*

ACU Dept. of Biology
Undergraduate Researcher in Dr. Qiang Xu lab, 2016-2017
Project: Analysis and detection of viral DNA within local mosquitoes

ACU Dept. of Biology
Undergraduate Researcher in Dr. Joshua Brokaw lab
Project: Formation and analysis of phylogenies of rat genus, *Thomasomys,* through DNA sequencing and analysis

Presentations and Publications

ACU Undergraduate Research Festival 2017
Poster Presentation
"Investigation of potential viral DNA and RNA genes in Abilene-area mosquitoes"

Evolution Conference 2016, Austin, TX
Poster Presentation
"Nuclear markers for phylogeny reconstruction in *Thomasomys* (Rodentia: Cricetidae)"

ACU Undergraduate Research Festival 2016
Poster Presentation
"Phylogeny of rodent genus *Thomasomys* (Rodentia: Cricetidae) based on the nuclear gene recombination activating gene 1"

ACU Undergraduate Research Festival 2015
Poster Presentation
"Patterns of D-loop sequence variation in *Thomasomys* (Rodentia: Cricetidae)"

ACU Undergraduate Research Festival 2014
Poster Presentation
"Reconstruction of phylogenetic relationships in *Thomasomys* (Rodentia: Cricetidae) based on cytochrome C oxidase subunit 1"